Advection pathways at the Mt. Cimone WMO-GAW station: seasonality, trends, and influence on atmospheric composition.

E. Brattich[1], J.A.G. Orza[2], P. Cristofanelli[3], P. Bonasoni[3], A. Marinoni[3], L. Tositti[4]

[1] Department of Physics and Astronomy DIFA, Alma Mater Studiorum University of Bologna, 40126 Bologna (BO), Italy.

[2] SCOLAb, Fisica Aplicada, Miguel Hernandez University, 03202 Elche, Spain.

[3] ISAC-CNR, Via Piero Gobetti, Bologna (BO), Italy.

[4] Environmental Chemistry and Radioactivity Laboratory, Department of Chemistry "G. Ciamician", Alma Mater Studiorum University of Bologna, 40126 Bologna (BO), Italy.

Corresponding author: Erika Brattich (erika.brattich@unibo.it)

Keywords: back-trajectories; teleconnection; trends; aerosol; atmospheric radiotracers.

Highlights:

- Characterisation of primary advection pathways to the Mt. Cimone baseline station
- Characterisation of atmospheric constituents by advection pathway to Mt. Cimone
- Trend analysis of atmospheric pathways and atmospheric composition at Mt. Cimone
- Associations between pathways, atmospheric composition and teleconnection indices

Abstract

Relationships are analysed between advection pathways and atmospheric composition at the high-mountain station of Mt. Cimone (Italy), between 1999 and 2006. Back-trajectory cluster analysis identifies eight main advection pathways. A connection is demonstrated between the seasonality of airmass transport and atmospheric composition. Temporal trends and correlation of variables, flow types and teleconnection indices show, among other, decreasing trends of ^{210}Pb (a radionuclide of crustal origin; -0.008 mBq m^{-3} year^{-1}) as well as PM_{10} (-0.15 µg m^{-3} year^{-1}), indicating that previously observed downward PM_{10} trends in Europe may actually be attributable to a combination of meteorological factors and decreasing anthropogenic emissions. The detection of a positive (negative) correlation of these tracers with Western (Arctic) air masses, showing significant downward (upward) trends at the study site, further confirms our findings. Lastly, relationships between teleconnection indices and atmospheric transport types/atmospheric variables are further analysed, focusing on large-scale atmospheric circulation indices and regional low-frequency atmospheric circulation pathways, the Mediterranean Oscillation and the Western Mediterranean Oscillation. The analysis reveals the important influence of such regional indices on the advection pathways.

1 Introduction

There is a pressing need to improve understanding of processes contributing the seasonal variability of background/baseline (i.e. well-mixed tropospheric) atmospheric composition in the central north Mediterranean region, a hotspot of air pollution and climate change. In fact, due to the sunny, hot and dry weather typical of this region especially during summer, together with the convergence of long-range transport over the basin, air pollution in the form of reactive compounds is often higher than in most European inland regions (Dulac et al., 2016). In addition, climate change will significantly impact air quality with numerous two-way interactions not always well understood.

Air pollution in the Mediterranean basin is primarily in the form of particulate matter and ozone and nitrogen deposition (Ochoa-Hueso et al., 2017).

In this framework, clustering of backward trajectories has been used to study the influence of the origin and pathway of air masses on composition change (for a review see Fleming et al., 2012). The investigation of vertical motions in the atmosphere may take advantage of using ^{7}Be and ^{210}Pb radiotracers, because of their naturally contrasting origin: in fact, ^{7}Be (half-life 53.3 days) is produced by cosmic ray spallation reactions with nitrogen and oxygen in the stratosphere (about 75%) and in the upper troposphere (Usoskin and Kovaltsov, 2008), while ^{210}Pb (half-life 22 years) is a tracer of continental air masses (Balkanski et al., 1993), being emitted as decay product of ^{222}Rn (half-life 3.8 days) deriving from crustal rocks and soils (Turekian et al., 1977). Once produced, both radionuclides attach to submicron-sized aerosol particles peaking in the accumulation mode (e.g., Gaffney et al., 2004). Thereafter, the main removal mechanisms of ^{7}Be and ^{210}Pb from the atmosphere are wet and dry scavenging of the carrier aerosol (Feely et al., 1989; Kulan et al., 2006). For this reason, simultaneous measurements of ^{7}Be and ^{210}Pb, and analysis of their ratio, can provide useful information about the vertical motion of air masses as well as on convective activity in the troposphere (e.g., Koch et al., 1996; Lee et al., 2007).

The use of air mass classification together with atmospheric radiotracers is not common, but has been the subject of some studies (e.g. Arimoto et al., 1999; Hernández et al., 2008; Dueñas et al., 2011; Lozano et al., 2012; Chambers et al., 2013, 2014, 2016 a,b; Grossi et al., 2016; Hernandez-Ceballos et al., 2016). However, most of the previous studies of this kind in the

Mediterranean region focused on relatively short time series, and focused on understanding the variability of atmospheric radiotracers without a clear connection to other atmospheric compounds. Moreover, while the relation between natural radionuclides and teleconnection indices has been the subject of recent studies (Grossi et al., 2016; Sarvan et al., 2017), the variability in the occurrence of each trajectory group and the assessment of trends in association with large-scale atmospheric circulation indices, such as the North Atlantic Oscillation index (NAOi), is less common (Orza et al., 2013). Even less studied is the association in the occurrence of advection pathways with the remaining modes of atmospheric circulation over Europe, such as the Eastern Atlantic (EA) pattern, Eastern Atlantic/Western Russia (EA/WR), and the Scandinavian (SCA) pattern. Together with NAO, these indices represent the most important mid-latitude modes for the Mediterranean climate at the monthly time scale (Trigo et al., 2006).

In this context, long-term measurements at the high-elevation WMO-GAW baseline station of Mt. Cimone (Italy; 44°11' N, 10°42' E, 2165 m asl) are of paramount importance. In particular, they are useful for the identification of dominant advection pathways, assessing associations between pathways and atmospheric composition, and investigating links between flow pathways and circulation modes in the Mediterranean region on seasonal and interannual time scales. In addition, the occurrence of trends and the relationships of trends in atmospheric composition with those in advection pathways and teleconnection indices in the monthly time series are also explored, focusing not only on large-scale indices but considering two additional regional low-frequency atmospheric circulation pathways, namely the Mediterranean Oscillation (MO) and the Western Mediterranean Oscillation (WeMO). It should be emphasized here that, historically, the investigation of atmospheric circulation model influences (both large-scale and regional) typically focused on precipitation and temperature pathways. To date, there has been limited exploration of the relationship between these modes and advection pathways/atmospheric composition.

This work is organized as follows. We first describe the measurement techniques and the statistical methods used. We then present and discuss our results on: 1) the description of the main advection pathways found by the cluster analysis of back trajectories; 2) the analysis of the relationships between advection pathways and meteorological parameters/other atmospheric components; 3) the temporal analysis of the monthly time series, including trends; 4) the associations of air flow types with teleconnection indices and meteorological/atmospheric variables. We finally summarize our main conclusions.

2 Materials and Methods

2.1 Sampling site

Mt. Cimone, the highest peak of the Italian northern Apennines, hosts a global station of the Global Atmosphere Watch (GAW) programme of the World Meteorological Organization (WMO) constituted by a meteorological observatory by the Italian Air Force (active since 1941) and a research facility managed by the Institute of Atmospheric Sciences and Climate (ISAC) of the National Research Council of Italy (CNR), active since 1996. The site is located far away from large industrialized and urban areas, has a 360° free horizon experiencing both regional and long-range transport of air masses (Bonasoni et al., 1999, 2000b; Cristofanelli et al., 2006, 2009a, b, 2013; Cristofanelli and Bonasoni, 2009; Tositti et al., 2013). The elevation of the site (2165 m asl) is such that the station lies above the planetary boundary layer (PBL) during most of the year, even if an influence of the innermost layer is evident during warm months due to the

increased mixing height and the influence of the mountain/valley breeze regimes (Fischer et al., 2003; Cristofanelli et al., 2007; Griffiths et al., 2014). For these reasons, under specific conditions (i.e. usually during cold months and during stable summer nights when regional anti-cyclonic conditions dominate), the measurements of atmospheric compounds and meteorological parameters at this site can be considered representative of the well-mixed southern European-Mediterranean basin free troposphere (Bonasoni et al., 2000a; Fischer et al., 2003; Cristofanelli et al., 2007, 2018), a region which is recognized as a hot-spot both in terms of climate change and air quality.

2.2 Measurements

As a WMO-GAW station, several atmospheric compounds have been measured at Mt. Cimone for many years (Cristofanelli et al., 2018): CO_2 (since 1979) (Ciattaglia, 1983, 1986; Colombo et al., 2000), tropospheric O_3 (since 1991) (Cristofanelli et al., 2015, 2018), concentration and size distribution of particles with optical diameter between 0.30 and 20 μm (since 2000) (Marinoni et al., 2008), black carbon (July 2005) (Marinoni et al., 2008), and CO (since 2007) (Cristofanelli et al., 2009b).

^{7}Be, ^{210}Pb and aerosol mass loading in the form of PM_{10} (airborne particulate matter with a mean aerodynamic diameter less than 10 μm) were measured regularly in the period 1998-2011 with a Thermo-Environmental PM_{10} high-volume sampler (average flow rate of 1.13 m^3 min^{-1} at standard temperature and pressure conditions) (Lee et al., 2007; Tositti et al., 2012, 2013, 2014).

After retrieval, the observations of the various atmospheric parameters previously mentioned, as well as of meteorological parameters such as temperature, pressure, relative humidity, and wind speed, were averaged to the same time resolution of PM_{10} and atmospheric radionuclides for statistical homogenization of data. In fact, as the PM_{10} filters at the station are manually changed, sampling time is not uniform. Anyway as most of the samples were collected over 48 hours (sampling approximately 3250 m^3 of air), in order to safely apply statistical techniques, data have been firstly homogenized by selecting only those samples which collected a volume between 2700 and 3700 m^3.

We also included tropopause heights in the analysis, calculated from the radiosoundings in San Pietro Capofiume (44°39'N, 11°37'E, 10m a.s.l.), a regional meteorological station located in the Po Valley to the North-East of Mt. Cimone, available since 1987 from the University of Wyoming website (http://weather.uwyo.edu/upperair/sounding.html).

2.3 Teleconnection indices

As reported in the Introduction, here we investigate the connection of atmospheric composition and advection pathways with teleconnection indices, considering both large-scale and regional scale teleconnections, i.e. NAO, EA, EA/WR, SCA, MO, and WeMO. Table 1 presents an overview of the teleconnections investigated in this paper.

The NAO, a redistribution of atmospheric mass between the Arctic and the subtropical Atlantic (Hurrell, 1995), has been identified as the dominant mode of variability of the surface atmospheric circulation across the Atlantic (Barnston and Livezey, 1997). The NAO is determined by the position and strength of the Icelandic low and the Bermuda-Azores High. Oscillations between high and low NAO phases modulate the westerly jet stream and cause large changes in the heat and moisture transport between the Atlantic and the neighbouring continents (e.g., Hurrell, 1995, 1996), affecting the intensity and number of storms (Hurrell et al., 2003). These changes influence air pollutant transport and dispersion, impacting, for instance, the

transport of Saharan dust into the Mediterranean and Atlantic in winter (Moulin et al., 1997), the export and import pathways of pollution to the Mediterranean basin (Hurrell, 1995), influencing local-to-regional scale pollutant concentrations (e.g., Cuevas et al., 2013; Cristofanelli et al., 2015), and modifying the transport of pollutants from North America to Europe (Li et al., 2002). A relation between the NAO phase and Stratosphere-to-Troposphere Transport (STT) variability has also been pointed out (James et al., 2003; Cristofanelli et al., 2006, 2015). A common measure of the NAO phase is the so-called NAO index (NAOi) which is commonly defined as the difference in normalized sea level pressure (SLP) anomalies between either Lisbon (Portugal) or Ponte Delgada (Azores), and Stykkisholmur/Reykjavik (Iceland) (Hurrell, 1995). Alternative definitions of NAOi have been introduced, including one based on the empirical orthogonal function (EOF) analysis of the SLP field. The NAOi in this case is identified as the leading eigenvector (the first Principal Component, PC1) computed from the time variation of the SLP field (e.g., Hurrell et al., 2003). The advantage of using EOF analysis of the SLP field is that the PC1 provides a more accurate representation of the NAO pattern considering the shifting of the NAO centres of action throughout the year (Pausata et al., 2012). This index appears to be less noisy than the station-based indices. Both monthly indices present a significant correlation coefficient equal to 0.80 and 0.76 over the periods 1998-2011 and 1999-2006 used in this work, respectively. Another alternative NAO index, the CRU station-based NAOi, is calculated as the difference between the normalised SLP over Gibraltar and the normalised SLP over southwest Iceland (Jones et al., 1997). CRU station-based index presents a significant correlation coefficient with the previous ones (equal to 0.79 with Hurrell station-based NAOi, and equal to 0.77 with Hurrell principal components-based NAOi).

The EA pattern is the second prominent mode of low-frequency variability over the North Atlantic, and was first described by Wallace and Guntzler (1981) as anomalously high 500 mb height anomalies over the subtropical North Atlantic and eastern Europe when in positive mode. It consists of a north-south dipole of anomaly centers spanning the North Atlantic from east to west. The positive phase of the EA pattern is associated with above-average surface temperatures in Europe in all months and it has been suggested to play a role in positioning the primary North Atlantic storm track (e.g., Seierstad et al., 2007) and in modulating the location and strength of the NAO dipole (Hurrell and Deser, 2009).

The EA/WR pattern (Lim, 2015) affects Eurasia throughout the year and consists of four main anomaly centers. The positive phase is associated with positive height anomalies located over Europe and northern China, and negative height anomalies located over the central North Atlantic and north of the Caspian Sea.

The SCA pattern (Bueh and Nakamura, 2007) consists of a primary circulation center over Scandinavia, with weaker centers of opposite sign over western Europe and eastern Russia/ western Mongolia. The positive phase of this pattern is associated with positive height anomalies, sometimes reflecting major blocking anticyclones over Scandinavia and western Russia, while the negative phase of the pattern is associated with negative height anomalies in these regions.

The MO is a low-frequency variability pattern producing opposing barometric, thermal and pluviometric anomalies between the western and eastern borders of the Mediterranean basin. The MO was originally defined as the difference of standardised geopotential height anomalies at Algiers (Alger) and Cairo (Egypt) (Conte et al., 1989), while similar indices have been defined in terms of the difference of standardised pressure anomalies at Gibraltar (Spain) and Lod (Israel) (Palutikof, 2003) or at Marseilles (France) and Jerusalem (Israel) (Brunetti et al., 2002).

It has a significant influence over rainfall in the Mediterranean basin (e.g., Martin-Vide and Lopez-Bustins, 2006; Angulo-Martínez and Beguería, 2012). The WeMO was defined within the synoptic framework of the Western Mediterranean basin and its vicinities (Martin-Vide and Lopez-Bustins, 2006). It is defined as the difference between the standardized surface pressure values in Padua (Italy), and San Fernando (Cadiz, Spain): while the north of Italy is an area with a relatively high barometric variability due to the influence of the central European anticyclone and the Liguria low, the gulf of Cadiz is often influenced by the Azores anticyclone. Similar to MO, WeMO has an important effect on precipitation in the Mediterranean, and especially in the eastern Iberian Peninsula (e.g., Martin-Vide and Lopez-Bustins, 2006; Angulo-Martínez and Beguería, 2012; Izquierdo et al., 2013), where NAO is weakly correlated with precipitation.

2.4 Clusters of back trajectories, significant differences and trends

In order to analyse the origin of air masses arriving at the measurement site, 96-hour 3D kinematic back-trajectories starting four times a day (00, 06, 12, 18 UTC) at three heights (1400, 2200 and 3000 m asl) were calculated with the HYbrid Single-Particle Lagrangian Integrated Trajectory (HYSPLIT) model version 4.8 (Draxler and Hess, 1997, 1998; Draxler, et al., 2018). A 96-hour time length was considered representative for long-range transport to the receptor site and to better control the uncertainty of back-trajectories. Sensitivity tests with a 6-day time length were also performed; however, their results indicate a reduced number of clusters with lower significant differences in atmospheric parameters and constituents, suggesting that these longer trajectories may lose part of their specific features.

The first issue faced in the calculation of the back-trajectories was the choice of the meteorological fields used as input, linked to the strongest source of errors (Stohl et al., 2001) when calculating back-trajectories, and eventually influencing the outcome of the trajectory clustering (Cabello et al., 2008a).

As previously observed in Brattich et al. (2017a, b), the coarse resolution of the terrain model included in the meteorological databases is generally not able to adequately resolve the topography of Mt. Cimone. In this work we used the National Center for Environmental Prediction (NCEP)/National Center for Atmospheric Research (NCAR) reanalysis with a 2.5° latitude-longitude resolution, 17 pressure levels from 1000 to 10 hPa, and 6 hourly data, which was the best compromise available at the time we started the back-trajectories calculation. Such a coarse resolution, too large to resolve mesoscale subsynoptic processes, is still acceptable for our study since we are most interested in the large-scale flow pattern more meaningful in a long-term quasi-climatological approach. The vertical motion of the air parcels was calculated from the vertical velocity fields. As a rule and due to the methodology applied to compute the back-trajectories (the computation uses the horizontal gradient of the field, calculated as a “centered difference” with meteorological data on a subgrid that follows the trajectory), it is recommended that trajectories at three heights are calculated simultaneously (see https://www.arl.noaa.gov/hysplit/hysplit-frequently-asked-questions-faqs/faq-hg23/). In this case, trajectories were calculated at 2200 m asl (just above the monitoring site), at 3000 m asl (800 m higher, at the edge of the free troposphere) and at 1400 m asl (above the terrain’s height for the measurement site in the model, to better consider meteorology below the study site). In the following, results are reported and discussed only for the height corresponding to that of the receptor site. The analysis at 3000 m, useful to compare the study site with the free troposphere, is included in Supporting Information (SI).

As for the association between trajectories and samples, each aerosol sample with its physico-chemical properties was associated with a specific advection pattern only if at least 60% of the calculated trajectories ending at the site during the sampling corresponded to that advection pattern. However, samples out of the outlined conditions were also analysed in depth with emphasis on flows characterized by fast and high-frequency variability often associated with singular though relevant trajectories (i.e. cutoff lows or Saharan dust incursions).

Clusters of back-trajectories were calculated following a clustering procedure based on the k-means algorithm, with specific features like the use of great-circle distances and determination of the number of clusters from the evaluation of the classification into k clusters (considering a large number of replicates), with k running from 15 to 3, (see for example Cabello et al. (2008b), Dueñas et al. (2011), Perrone et al. (2013), Brattich et al. (2016)). Significant differences in the analysed meteorological and atmospheric parameters according to the identified clusters were analysed using the Kruskall-Wallis test, without any "a priori" assumption of their distribution (Brankov et al., 1998). Whenever significant differences among the groups were found, pairwise Mann-Whitney tests were performed to identify the significantly different pairs. Conservatively, p-values in the latter were compared against adjusted significance levels α using the Dunn-Sidák correction for multiple comparisons $\alpha = 1 - (1 - \alpha_t)^{1/n}$, where $n = k\,(k-1)/2$ is the number of pair-wise comparisons done between k categories, with overall significance $\alpha_t = 0.05$.

Composite synoptic charts of 700, 850 and 1000 hPa geopotential height, computed with data from NCEP/NCAR re-analysis project database (Kalnay et al., 1996), available from the Earth System Research Laboratory, Physical Sciences Division, of the USA National Oceanic and Atmospheric Administration (NOAA) at http://www.esrl.noaa.gov/psd/ were used to analyse the meteorology of individual situations.

The presence of trends in the monthly time series over the study period considered in this work was examined though a number of nonparametric statistical methods, mainly based on the Mann-Kendall (M-K) tau test to assess the significance of monotonic trends and the Theil-Sen (T-S) slope estimate for trend magnitude. In particular, considering that the significance of a trend is affected by the presence of serial correlation, and, conversely, the estimate of the serial correlation is also altered by the presence of a trend, the correlation coefficients at different lags were first estimated by computing the sample autocorrelation function (ACF) for each time series. The results indicated that, in general, the analysed time series present some degree of serial correlation, together with seasonality; as a consequence, two methods of trend analysis have been used with the aim of removing, or reducing, the influence of seasonality and lag-1 autocorrelation in the monthly data:

(1) The seasonal Kendall test (Hirsch et al., 1982), which applies the M-K trend test separately for each month and then combines the results. (2) The trend-free pre-whitening (TFPW) procedure (Yue et al., 2002) applied to the seasonally adjusted monthly time series, to remove the influence of the month-to-month correlations in the significance of the trends. The TFPW procedure comprises several steps, including the linear detrending of the time series using the T-S slope, the removal of the serial autocorrelation of the residuals and the add-back of the discarded linear trend to the remaining time series, before the M-K test is applied. Seasonal-trend decomposition of the time series was used to obtain the de-seasonalized time series, which were subsequently analysed by the TFPW procedure. The decomposition technique used in this work (STL decomposition hereafter) is based on LOESS (locally weighted low-degree polynomial regression), a nonparametric regression technique recursively applied to the seasonal and trend

components (Cleveland et al., 1990). Additionally, the resulting (nonlinear) trend component has been used for the visual assessment of the long-term behaviour of the time series.

The association between the frequency of each advection pattern and observations at the sampling site, as well as with the NAOi and other large- and regional-scale teleconnections, has been examined for the de-trended monthly time series and for the seasonal means via least-square regression analysis with statistical significance evaluated by a two-tailed *t*-test. Since relationships are not necessarily linear, the nonparametric Kendall rank test has also been used to identify any statistically significant association without any "a priori" assumption of their form. Spearman correlation coefficients have been computed for the cases with significant association.

3 Results and discussion

3.1 Characteristics of the main advection pathways

Figure 1 shows the centroids (representative trajectories) of the 8 clusters obtained at 2200 m asl and the relative percentage frequency of each flow pattern over the whole 1998-2011 period, together with the mean height evolution over time and the monthly variation of the frequency of the air flow pathways reaching the receptor site.

Cluster names were chosen based on their region of provenance. Most of the trajectories correspond to westerly flows; in particular, westerly trajectories are classified into Northern Atlantic (N Atl), North America (N Am), Atlantic (Atl), Western (W), and North-Western Europe (NW-Eu) flows, together representing more than 60% of the flows. The remaining trajectories are classified into Arctic (A), Eastern (E), and Mediterranean-Africa (Me-Af).

As from the mean height evolution over time of the representative trajectories reported in Figure 1, the Arctic and North-American trajectories descend from the most elevated heights while approaching the site, and eventually rise again and cross over the Alps. North Western-Europe and Eastern flows do not considerably change their height during their transport, whereas Western, Atlantic and (more specifically) Mediterranean-Africa trajectories generally reach the observatory from very low levels.

Figure 2 shows the box plots of meteorological parameters, i.e., pressure, temperature, relative humidity, precipitation, tropopause height, wind speed, and mixing height by advection pattern. Similar to Figure 2, Figure 3 depicts box plots for the atmospheric species, such as O_3, CO_2, BC, CO, fine and coarse particles, PM_{10}, ^{7}Be, and ^{210}Pb, associated with each flow pattern at 2200 m and at 3000 m asl. Additionally, the analysis extends over nuclidic and mass ratios such as $^{7}Be/^{210}Pb$, $^{7}Be/PM_{10}$, $^{210}Pb/PM_{10}$, used to gain insights into the vertical motions of air masses as well as on convective activity in the troposphere (e.g., Koch et al., 1996), are also analysed. The summary statistics together with significant differences of each variable by advection pattern is reported in the SI. In order to better characterize the flow pathways, both boxplots and summary statistics refer to the "pure cases", i.e., the samples attributed to only one advection pathway (when at least 60% of the trajectories ending at Mt. Cimone during one single sampling period belong to the same advection pathway).

Below we summarize the major characteristics of the identified advection pathways in terms of seasonal variability, mean height, meteorological variables and atmospheric composition, as indicated in Figures 2 and 3.

- A: advection of fast and elevated (mean height of the cluster equal to 3113 m) air masses originating in the Arctic/polar regions. This trajectory type is more frequent in autumn and winter. This subsiding air flow is associated with low temperatures, low relative humidity, low wind speeds, relatively low values of the tropopause height (probably due

to the fact that these air masses are not vertically thick compared to other air masses), and moderate mixing heights. Such air masses can be linked to the presence of lows or cut-off lows characterized by low tropopause or tropopause folding and in fact are also associated with rather low pressure systems. Due to their subsiding nature, travelling at high altitudes over remote regions, these air masses are generally moderately clean, i.e. associated with low values of O_3, black carbon, CO, PM_{10}, and ^{210}Pb. It is also associated with high ^{7}Be and therefore with high $^{7}Be/^{210}Pb$ and $^{7}Be/PM_{10}$. This kind of transport is in fact frequently associated with STE, in agreement with previous observations of stratospheric intrusions at Mt Cimone (Bonasoni et al., 1999, 2000a, 2000b; Brattich et al., 2017a). In particular, the high ^{7}Be, $^{7}Be/^{210}Pb$ and $^{7}Be/PM_{10}$ can be attributed to the high production rate of ^{7}Be in the stratospheric air at high latitudes (Beer et al., 2012), , even though the reduced ozone concentration points out a connection with subsidence from the upper troposphere, a region connected with increases in ^{7}Be but not in O_3.

- E: advection of relatively slow and low (mean height equal to 2190 m) air masses from East. This flow type is more frequent in April, May and September, and groups the 13% of the trajectories. These air flows are associated with low tropopause height, while pressure, wind speeds, humidity, and mixing height take intermediate values. This flow type brings lower concentrations of PM_{10} than the Western advection, but is associated with higher loadings of fine than coarse particles, in agreement with observations by Tositti et al. (2013). This flow type is also associated with moderately high black carbon and high ^{210}Pb, and to the lowest values of $^{7}Be/^{210}Pb$ activity ratio; overall this flow can be labelled as "continental polluted".
- Me-Af: relatively short and low (mean height equal to 2154 m) Mediterranean and North-African air masses. These trajectories, grouping the 18% of the total, are active all-year round but mainly in spring and autumn. These flows cross over the Mediterranean at low altitude and correspondingly are warm and humid, and are associated with low wind speeds and intermediate mixing height (close to 1400 m, which is below the typical mean height reported for Saharan dust transport, between 1500 and 4000 m asl; see Jorba et al., 2004 and Papayannis et al., 2008). These air masses bring substantial PM_{10} loadings as linked to Saharan Dust transport (in agreement with Duchi et al., 2016), associated with increases in both fine and coarse sized particles. It contributes also to BC and to high ^{210}Pb and ^{7}Be concentrations, and thus to rather low $^{7}Be/^{210}Pb$, $^{7}Be/PM_{10}$ and $^{210}Pb/PM_{10}$ ratios. Overall, this flow may be labelled as "African convective", including the often-observed biomass burning tracers. In particular, similar to what Dueñas et al. (2011) and Brattich et al. (2017a) reported, Mediterranean-Africa air masses are linked to high activities of both ^{7}Be and ^{210}Pb, due to the combination of downward transport from the upper troposphere and African dust uplifting.
- W: advection of relatively slow and low-level (mean height equal to 1915 m) air masses from West, which are active all year round but are more frequent in July, August, and October. This flow pattern groups the 15% of the trajectories. These air masses are associated with high pressures, high temperatures, low relative humidity, high tropopause height, moderate wind speeds, and moderate-to-high mixing heights. This advection pattern carries elevated values of O_3, PM_{10}, fine and coarse particles; it contributes to a large degree also to black carbon, a tracer of combustion. This is likely related to of the entrainment of aged, polluted air masses into this flow type when crossing coastal areas in the western Mediterranean. It contributes also to high ^{210}Pb and ^{7}Be concentrations

(low $^{7}Be/PM_{10}$, $^{210}Pb/PM_{10}$ and $^{7}Be/^{210}Pb$ ratios) suggesting associated convective pathways.

- Atl: relatively fast and low-level (mean height equal to 1974 m) air masses coming from the Atlantic Ocean. This advection pattern is most common from October to April. It groups only the 8% of the trajectories. These air masses are moderately warm and humid, present low pressure levels, moderate to high wind speeds, and low mixing heights. This advection pattern shows low contributions of O_3, black carbon, PM_{10}, ^{7}Be and ^{210}Pb, as a consequence of the renewal of air masses by these strong mid latitude maritime flows and the relatively high wind speeds recorded at the site.
- N-Am: polar fast and upper level (mean height of the cluster equal to 2965 m) air masses that originate as continental air over North America. This air mass type is negligible in summer months, mostly occurring from October to April. This advection pattern is the least frequent among those emerged for Mt. Cimone (5% of the trajectories arriving at the receptor site). Similar to the Arctic type, these are cold, dry subsiding flows. They are related to the lowest temperatures (even lower than the Arctic ones), lowest pressure levels, low relative humidity, low tropopause heights and mixing heights, and moderate wind speeds at the study site. The polar-front jet stream is present at upper levels. North American air masses are usually very clean (low in O_3, black carbon, CO, PM_{10} as well as in both fine and coarse particles), with the lowest mean and median values of these species. The cleanliness of these flows derives from their subsiding nature originating quite high above the North American region, and reaching Mt. Cimone (i.e. southern Europe) at moderately high wind speeds. This results in the replacement of air masses with cleaner, fresh air, as previously observed also at other southern Mediterranean sites in Spain and Italy (e.g., Cabello et al., 2008b; Perrone et al., 2013, 2014). Also the atmospheric radiotracers ^{7}Be and ^{210}Pb present low concentrations within this flow type, probably due to the low concentration of suspended fine particles and relatively younger upper level air masses.
- N-Atl: relatively fast, but not very high (mean height of the cluster equal to 2562 m) air masses coming from the Northern-Atlantic Ocean. Active throughout the year with highest frequency in July. This group of trajectories comprehends the 14% of the total. These air masses are moderately warm, very humid, and connected to slow wind speeds and high mixing height. This flow pattern shows elevated contributions of O_3 and fine particles, but low values of black carbon , carbon monoxide and ^{210}Pb, while it contributes moderately to PM_{10} and ^{7}Be (low $^{7}Be/PM_{10}$, $^{210}Pb/PM_{10}$ and $^{7}Be/^{210}Pb$ ratios), probably due to contribution of aged pollutants from Western Europe where they travel after their residence over the North-Atlantic Ocean, in agreement with Brattich et al. (2016).
- NW-Eu: slow and not very high (mean height equal to 2321 m) continental air masses coming from North Western-Europe. This flow pattern, with mean height equal to 2321 m, is more frequent in summer months and groups the 19% of the trajectories. These air flows present the lowest wind speeds and high pressures, frequently related to blocking situations in the summertime; they are also related to high temperatures, relative humidity and mixing height. Similar to the Eastern advection, it brings lower concentrations of particulate matter with respect to the Western flow type, but associated with higher loadings of fine particles than coarse ones. These flows contribute moderately, together

with Eastern air masses, to black carbon and to high ^{210}Pb (low $^{7}Be/PM_{10}$, $^{210}Pb/PM_{10}$ and $^{7}Be/^{210}Pb$ ratios).

3.2 Atmospheric parameters by advection pattern

The large-scale advection pathways found at Mt. Cimone have been described in terms of meteorological variables and atmospheric composition in the previous subsection. Summarizing, North Atlantic and NW Europe advections, both passing over the British Isles and France, present the highest O_3 levels. In turn, Atlantic as well as North America and Arctic air flows are associated with low O_3 values, which points out the influence of precursor levels. CO_2, a long-lived greenhouse gas, is well-mixed in the free troposphere and not much affected by the boundary layer dynamics, with values homogeneously distributed over all the flow types. While Mediterranean Africa and Western air masses are associated with high number of both fine and coarse particles, as related to the transport of marine and desert particles together with anthropogenic pollution, North Atlantic advections are high only in fine particles related to the transport of polluted particles from anthropogenic origin.

Low values of the ^{210}Pb crustal tracer are observed when air masses arrive from the ocean (Atlantic, North Atlantic and Northern America) as expected, while ^{210}Pb maxima are linked to flows with an explicit continental origin such as Mediterranean-Africa, Western, Eastern and North Western-Europe. This behaviour is of course due to ^{210}Pb continental origin, as ^{222}Rn flux from the oceans into the atmosphere is negligible due to its low marine source (low radon emission) (Balkanski et al., 1993; Baskaran, 2011). ^{7}Be low values are connected to Atlantic and Northern American air masses, while Western flows are related to the highest values, likely connected to Gulf of Genoa and Gulf of Lion cyclogenesis, which have been long recognized as associated with STE (e.g., Stohl et al., 2000; Aebischer and Schär, 1998).

Here it is worth noting that due to the coarse resolution of the meteorological field we are using, our methodology is not able to resolve mesoscale and subsynoptic processes. However, such processes may have important effects on the variability of the atmospheric species we are considering. In particular, some of the identified advection pathways (the local and regional transports) can be associated with favourable “stagnation” conditions (mostly during the summer months), such as the increase in height of the regional PBL and/or mountain/valley breeze regimes, as previously investigated by Cristofanelli et al. (2013, 2016).

Figures 4 and 5 analyse the connection of the seasonality of advection pathways with that of radiotracers and PM_{10}, respectively. The seasonality of variables was analysed considering monthly medians as the distributions of PM_{10} and of atmospheric radiotracers are decidedly non-Gaussian (Tositti et al., 2013, 2014), and in this case the median should be preferred over the arithmetic mean as a more robust indicator (e.g., Wilks, 2011).

As shown in Figure 4 and as previously highlighted (Tositti et al., 2014; Brattich et al., 2016, 2017a), the seasonal behaviour of ^{210}Pb is characterized by the presence of one summer maximum mainly due to higher mixing height and enhanced uplift from the boundary layer. Conversely, ^{7}Be seasonal variations are more complex, being characterized by two relative maxima, one during the cold season (March) associated with an increased frequency of STE (James et al., 2003; Stohl et al., 2003; Brattich et al., 2017a) and one in the warm season mainly (but not exclusively) associated with tropospheric subsidence balancing low tropospheric air masses uplift generated by the convective circulation produced by the intense solar heating and the higher tropopause height increase of this season (Ioannidou et al., 2014), occasionally accompanied by STE (Cristofanelli et al., 2009a; Tositti et al., 2014). Figure 5 highlights,

however, that the seasonality of radionuclides can also be connected to the seasonality of air mass transport at the site, as previously pointed out by Brattich et al. (2017b) by means of model simulations with a Chemistry and Transport Model. In fact, while ^{7}Be March maximum seems to be related to the seasonal pattern of Arctic air masses (as Atlantic and North American air masses, presenting also a simultaneous winter peak, are associated with lower ^{7}Be values in the boxplots of Figure 3), the ^{7}Be summer maximum seems to correspond to that presented by Mediterranean-Africa, Western and North Atlantic air masses. ^{210}Pb summer maximum seems instead to be well related with the seasonality of Western and North Western-Europe flows. However the monthly analysis is not capable of resolving the contributions of advection pathways occurring in the same month and therefore to uniquely determine a clear connection between advection pattern and concentration.

Figure 5 provides similar analyses for the PM_{10} seasonal pattern, which, like ^{210}Pb, show minimum values during the cold season and maxima during summer months, when it is uplifted from the regional boundary layer due to thermal convection and increased mixing height (Tositti et al., 2013). The seasonal pattern of PM_{10} might be, however, influenced by the seasonal pattern of advection pathways bringing about elevated mass loads of particles, such as Mediterranean-Africa, Western, North Atlantic and North Western-Europe air masses. In particular, while the seasonal maximum frequency of Mediterranean-Africa in June contributes to the first PM_{10} increase observed during this month, July values are related to the contribution of North Atlantic flows, and August elevated values are linked to the seasonal pattern of Western and North Western-Europe advections. Figure 6 also shows that the magnitude of the peaks is determined by both the source of trajectories and the concentration over source regions, as indicated by the analysis of the time spent by trajectories over North Africa together with the aerosol optical depth (AOD) over Africa from MODIS Aqua 5.1 collection (Deep Blue AOD at 550 nm). We have found that trajectories spend more time over northern Africa in November than in May, but AOD in Africa is lower in November (mean equal to 0.125 in November vs. 0.396 in May), an observation consistent with the low PM_{10} concentration in November. Similarly, the AOD at 550 nm (Land and Ocean) along the western Mediterranean shows higher values for May than for November (0.27 vs. 0.14).

Though the seasonal frequency of events accounts for most of the variability, a detailed analysis shows that singular events may make important contributions to some of the parameters observed. For this reason, Figure 6 reports boxplots of the median ^{7}Be/^{210}Pb contribution per number of episodes for each season. Figure 8 highlights that both summer Arctic as well as summer North-American flows, though being infrequent, can contribute to increases in ^{7}Be (and not in ^{210}Pb). Their average contribution to high ^{7}Be/^{210}Pb during summertime is higher than during winter when they are more frequent. Figure 8 also emphasizes Arctic, North Atlantic, North-American and Western flows as the main contributors to winter ^{7}Be/^{210}Pb increases; Mediterranean-Africa flows are instead associated with expectedly large contributions of ^{210}Pb and PM_{10}, while less obvious, but in agreement with previous studies (Hernández et al., 2008; Menut et al., 2009; Dueñas et al., 2011; Gordo et al., 2015), is the inherently high contribution in ^{7}Be. The high ^{7}Be of this flow type can be connected to the intense convection generated by the extremely high temperature of the ground and the very dry conditions in the Sahara desert together with the mineral dust size spectrum including also a large fraction of submicron particles to which ^{7}Be attaches (Brattich et al., 2017a). This confirms how, given the suitable dynamical framework, the ^{7}Be/^{210}Pb ratio is a pragmatic and efficient proxy of vertical motion.

3.3 Trend analysis of transport pathways, teleconnection indices and atmospheric composition

The assessment of the existence of temporal trends in the time series of the monthly frequencies of the air flow types, as well as of monthly medians of the variables and of teleconnection indices has considered the presence of seasonality and serial correlations in the time series (see SI). Indeed, as previously reported in the Methodology section, the analysis of the pattern of the ACF (AutoCorrelation Function) can reveal the presence of seasonality in the time series. Here, the previously described seasonal nature of the advection pathways, as well as of the analysed atmospheric variables, is also evidenced by the periodic behaviour of the ACF of their monthly frequencies of occurrence (in the case of advection types) and monthly medians (in the case of atmospheric species), with maxima and minima beyond bounds of significance (95% confidence) and a full cycle of 12 months. Examples of ACF are reported in the SI. In all cases the use of the STL (Seasonal and Trend decomposition using Loess) decomposition allowed the estimation of the relative contributions of the seasonal, trend and residual components, and the subsequent removal of the periodic structure (connected with the seasonal component) in the ACF for further analysis.

Since significant data loss occurred for technical reasons in 2007, the trend analysis was restricted only to the 1999-2006 time window. Although this time period is too short to provide definitive trend assessment, this analysis can provide useful hints as to the role of specific processes (e.g. meteorology vs anthropogenic emissions vs atmospheric transport) in modulating the variability of the atmospheric species. In addition, considering the decreasing number of samples towards the end of the time series and the consequent decrease in the number of trajectories, for the analysis of trends we considered the corresponding fraction of each trajectory type with respect to the total number of trajectories in a month. At this step of the research we also included in the analysis the tropopause height data obtained obtained from the Aqua AIRS satellite, available since August 2002 from the NASA Goddard Earth Sciences Data and Information Services Center (http://mirador.gsfc.nasa.gov/). The comparison of the tropopause height from radiosoundings and from satellite observations yields a strong significant correlation ($R^2 = 0.83$ for the monthly means and $R^2 = 0.71$ for the monthly medians).

Trend analysis on air flow pathways reveals some significant tendencies though of limited extent and also with some differences according to the different approaches applied, in particular seasonal Kendall test and trend-free pre-whitening methods (see Table 2). Both methods consistently detect significant trends in a number of cases, in particular indicating an increasing trend for Arctic flows and a decreasing one for Western flows. The seasonal absence of both Arctic and North-American flows strongly biases the Theil-Sen slope to zero. However, the seasonal Kendall tests suggest the presence of a significant trend in the Arctic time series, and deseasonalization provides a better estimate of the upward trend, As for the variables, the results indicate a strong upward trend for CO_2, in agreement with the long-term CO_2 behaviour at the global scale (Machta, 1972; Thoning et al., 1989; Randerson et al., 1997; WMO-GAW, 2017), and a significant decreasing trend for both the monthly medians of ^{210}Pb and PM_{10} measured at the station in the period 1999-2006 (Figure 7). The mean annual change of the original monthly time series is equal to +1.80 ppm $year^{-1}$, -0.008 mBq m^{-3} $year^{-1}$ and -0.15 μg m^{-3} $year^{-1}$, for CO_2, ^{210}Pb and PM_{10} respectively, while for the de-seasonalized monthly series it is equal to +1.90 ppm $year^{-1}$, -0.01 mBq m^{-3} $year^{-1}$ and -0.30 μg m^{-3} $year^{-1}$.

The detection of contemporary decreasing trends of ^{210}Pb and PM_{10} is particularly important in light of the decreasing trend of PM_{10} in the period late 90's-2010 observed in many stations in Europe, especially at regional background stations (Pérez et al., 2008; Barmpadimos et al., 2011; Colette et al., 2011; Barmpadimos et al., 2012). Generally, this PM_{10} drop is

attributed both to a decrease in anthropogenic emissions, as a result of to the mitigation strategies adopted, as well as to different meteorological processes or cycles, such as the frequency and intensity of Saharan dust episodes (Pérez et al., 2008). Both Colette et al. (2011) and Barmpadimos et al. (2012) showed that the decrease in anthropogenic emissions seems to be more important than meteorology as a driving factor for the observed decrease. However, in our case the observation of a contemporary decreasing trend of the ^{210}Pb radionuclide at this remote background site, which cannot be ascribed to a decrease in anthropogenic emissions due to the crustal natural origin of this nuclide, highlights the important role played by meteorology in these decreases.

A visual inspection of the time series and their trend components obtained from the seasonal-trend decomposition analysis (Figure 7) suggests that the upward trend of Arctic flows was significant from 2002 on, while Western flows downward trend was almost constant over the 1999-2006 study period. While CO_2 presents an upward trend over the time period, in agreement with, e.g., WMO-GAW global analyses (2017), for ^{210}Pb and PM_{10} the decreasing trend is stronger after 2001. Besides parameters characterised by the existence of significant trends, we also reported results for the two NAO indices with the aim of illustrating the result for this well-known and often studied teleconnection index, showing a slightly decreasing non-significant trend.

The increase in ^{210}Pb activity from 2002 to 2003 might be due to the extremely high temperature recorded in the whole European region, especially during the summer months (Cristofanelli et al., 2009a; Pace et al., 2005), and connected also to anomalously high ozone concentrations at Mt. Cimone (Cristofanelli et al., 2007) and to augmented radon exhalation during the 2003 summer heat wave in Europe. In PM_{10} this increase is masked by the 2004 maximum connected to an exceptional Saharan dust episode previously described (Beine et al., 2005) which resulted in an event concentration reaching 80 $\mu g\ m^{-3}$and characterized by a significant increase in the coarse fraction and a reduced, though not negligible, increase in the fine fraction (to which radionuclides attach), and with a less substantial increase in ^{210}Pb than in PM_{10} (Tositti et al., 2013; Brattich et al., 2015a, b).

The analysis of the two tropopause height datasets shows no trends at Mt. Cimone, contrarily to the increasing trend observed globally and suggested as an alternative detection variable of climate change (e.g., Añel et al., 2006), connected to the increase in atmospheric CO_2 leading to tropospheric warming and stratospheric cooling, and to anthropogenically induced depletion of stratospheric ozone, also inducing stratospheric cooling (e.g., see Chapter 5 of WMO, 2007; Myhre et al., 2013; Santer et al., 2013). The absence of trends in our case is possibly due to the different and short time window we use.

Both of the NAOi time series (the station-based and the Principal Components-based) do not show any significant trends according to the tests, despite presenting a negative T-S slope. For the sake of completeness, we also investigated the results for the CRU station-based NAOi which indicate the absence of statistically significant trends during the analysed period. The only teleconnection index presenting a significant trend during the study period is the WeMOi, with a downward trend constant over the study period. The downward trend is particularly evident in 2005 and 2006 in correspondence with very large negative indices indicative of the presence of strong lows in the Gulf of Cádiz and anticyclones in central Europe and associated with an increase of humid airflows travelling over the Mediterranean Sea and a reduction of westerly-northwesterly flows.

The analysis of the magnitude of the seasonal and trend components of the time series revealed that the seasonal component dominates over the trend component and the small-time scale variations in almost all the measured atmospheric variables, weighting about twice the trend component. In turn, the small-scale variations dominate most of the teleconnection indices with the exception of MOi, and the frequencies of the different advection pathways.

3.4 Association among air flow types, meteorological/atmospheric parameters and teleconnection indices

In this work, the degree of association among air flow types, meteorological/atmospheric parameters and teleconnection indices is assessed by analyzing the Spearman correlation coefficient, considering both the complete yearly time series and separately by season.

Figure 8 shows the linear Spearman correlation coefficients between teleconnection indices and flow types, while comprehensive tables with all the correlation coefficients are reported in the SI.

The NAO is related to North-American flows (especially in winter), and weakly related to Mediterranean-Africa (during summer and all-yearlong) and North-Atlantic pathways. It is recognized that the positive NAO phase corresponding to a stronger than usual subtropical high-pressure centre and deeper than normal Icelandic low results in more and stronger winter storms crossing the Atlantic Ocean on a more northerly track, while the negative phase is connected to fewer and weaker winter storms crossing on a more west-east pathway (Barnston and Livezey, 1987). An anti-correlation of westerly flows reaching three Mediterranean sites (Lecce, Elche and Malaga) with NAOi was previously observed by Orza et al. (2013): this observation is connected with the fact that the position of the subtropical high at lower latitudes during the negative phase of the NAO promotes the access of westerlies (W)/southwesterlies (Me-AF) to the Mediterranean. This is shown in Figure 9, presenting for each spatial grid cell the ratio between the residence time of the air parcels reaching Mt. Cimone during the positive and the negative phases of NAO (NAOi higher than +0.5 and lower than -0.5, respectively) for the extended winter period (DJFM), calculated as the number of trajectory endpoints falling within each area of interest divided by the total number of trajectory endpoints for the entire set of trajectories in the considered time period.

Figure 9 reveals that south-westerlies and slower westerlies from the westernmost part of Northern Africa and southern Spain are more frequent during the negative phase of the NAO, while flows from Libya and surrounding regions (also belonging to the Mediterranean-Africa cluster) occur preferentially during the positive NAO phase. Moreover, trajectories coming from North-America are more frequent during the positive phase of NAO, as indicated by the significant high correlation between North-American flows and NAO. Finally, North-Eastern flows seem to be more usually observed during the positive NAO phase, even if this was not readily observed from the correlation analysis.

The frequencies of Atlantic, North-Atlantic, North-American and Western flows are related to the WeMOi. In particular, while Atlantic, North-American and Western flows are related to the WeMOi both all-yearlong and during separate seasons specific for each advection pattern, the frequency of North-Atlantic trajectories is strongly connected with WeMOi in summer, and less so considering the whole time series. It is also weakly negatively related to the Eastern advection pattern. These correlations can be easily understood considering that this index measures the difference between the standardized surface pressure values measured in Padua

(Italy), and San Fernando (Cadiz, Spain). Therefore, these results suggest a likely connection of the downward trends of Western flows with WeMOi as previously observed.

MOi presents weak relations with Western and North-Western Europe pathways, and with North-American flows during winter. Also these relations can be easily understood from the MOi construction as the difference of standardised geopotential height anomalies at Algiers (Alger) and Cairo (Egypt).

EA, consisting of a north-south dipole of anomaly centres displaced South-Eastern with respect to the NAO ones, appears negatively related to Arctic flows (especially in autumn, and secondarily in winter and all-yearlong), and positively associated with Western (mostly in winter) and Atlantic flows (not in spring). Its relation with Me-AF has only a winter nature.

EA/WR and SCA indices present less relations with air mass pathways, probably due to their limited influence in central Europe; in fact, the EA/WR presents an association with Western flows only during autumn, while the SCA pattern is negatively correlated with Western, Atlantic, North-American and North-Atlantic pathways during winter, while positive associations with North-American and Western flows are observed during summer and autumn, respectively.

Figure 10 similarly reports the correlation coefficients between teleconnection indices and the monthly medians of and atmospheric composition variables.

The positive correlation of NAO during the transition seasons with particles concentration, even though not statistically significant, is linked to the fact that the positive NAO phases are associated with drier weather conditions in the Mediterranean area which generate intense uplift of particles from the ground; on the contrary, the negative correlation between the station-based NAOi and coarse particles is linked to their transport from Western and Mediterranean-Africa, and to a lesser extent from North Western-Europe flows, and to the association of the negative NAO phase with more westerlies/south-westerlies entering the Mediterranean. The association of the PC-based NAOi to O_3 during summer is in agreement with the results of Pausata et al. (2012) and is linked to the drier conditions in the Mediterranean area associated with the positive NAO phase resulting in the build-up of O_3 because of photochemical processes; however, the transport of O_3 enriched air masses from the Atlantic Ocean, where O_3 build-up is linked to the low dispersion capacity of precursors, increase of the photochemical yield and of kinetic reactions due to the high temperature, cannot be completely ruled out. In particular, Pausata et al. (2012) associated the O_3 increase in south-western Europe to transport of air masses from continental Europe, favoured by the presence of a more extended Azores anticyclone. In the case of Mt. Cimone, we observed an increase of Me-AF transport linked with the positive NAO phase. As such, the positive correlation of O_3 with NAOi could be linked to the role of mesoscale circulations (enhanced vertical transport and photochemistry under anticyclonic conditions) which are not resolved in our study due to the coarse resolution of the meteorological field we are using. The index showing the highest number of significant correlations with the variables is the MOi (both indices). In the MO positive phase, when higher pressures are found over the western and central Mediterranean, the storm track is displaced northward and the orientation of the westerly airflows is modified. This causes dry conditions in the Mediterranean basin, with low precipitation and relative humidity. Conversely, low pressures and in particular cyclogenesis over the western/central Mediterranean, which are linked to the negative MO phase, are associated with precipitation and high $^{7}Be/^{210}Pb$ and $^{7}Be/PM_{10}$ ratios.

Figure 11 reports the associations between monthly medians of the variables and frequencies of air flow types during different seasons as well as throughout the year. Most of

these associations agrees with Figure 3. Amongst the correlations observed, it appears particularly important and interesting to discuss those likely to be connected with the ^{210}Pb and PM_{10} negative trends observed in the previous section: Arctic flows, presenting an upward trend, are negatively related with ^{210}Pb and PM_{10} (all year-long, even though a positive relation during winter season also appears), while Western flows, presenting a downward trend, are positively associated with ^{210}Pb and PM_{10}. The anti-correlation of Arctic flows with ^{210}Pb and PM_{10} is mainly related to the continental origin of ^{210}Pb and PM_{10}, in agreement with Brattich et al. (2016, 2017b). In the Supplementary Material, tables reporting all significant correlation coefficients between teleconnection indices/advection pathways and variables are reported.

4 Summary and conclusions

This work focused on finding relationships between the advection pathways and atmospheric composition observed in a long time series of essential climate variables (ECVs) observed at the WMO-GAW station of Mt. Cimone (Italy). Advection pathways were identified by a cluster analysis of back trajectories starting at Mt. Cimone at three different heights; the cluster analysis identified 8 groups at the initiation height of 2200 m, approximately at the height of the station. The results reflect strong seasonal pathways with prevalence of westerlies as typical of mid-latitude Northern Hemisphere sites. The main features of these flow pathways, both from the meteorological and from the atmospheric composition point of view, were analyzed. The results indicate that North-American air masses, associated with subsiding flows originating at high altitudes, are related to low pressures and tropopause heights, cold, and dry air masses, and linked to high wind speeds. These flows are negligible during summertime, besides being related to low concentrations of atmospheric pollutants such as BC, CO, O_3, PM_{10}, but also of atmospheric radionuclides ^{7}Be and ^{210}Pb. Arctic flows are typically cold (though less than North American ones) and more frequent in the cold season. Being subsiding flows and travelling at high altitudes over remote ocean and ice, they are also connected to low values of atmospheric pollutants such as CO, O_3, BC, but also of particulate matter and ^{210}Pb. On the contrary, but for the same reason, this flow type is associated with high ^{7}Be and seems connected to SI events. Continental flows from North-Western Europe, Eastern Europe, Western and Mediterranean-Africa are generally linked to higher values of atmospheric components; in particular, NW-Europe, Western and Eastern flows are related to "pollution" events, being associated with high levels of CO, BC, O_3 and fine particles number densities, leading to corresponding increases in PM_{10}. In those cases, the relatively "short" back-trajectories suggest the occurrence of meteorological conditions characterised by low ventilation that, especially during warm months, can also promote the diurnal-scale transport of PBL air-masses to the receptor site (Cristofanelli et al., 2017). Because of their continental origin, these flows are also associated with high ^{210}Pb levels. Mediterranean-Africa flows associated with Saharan Dust events bring about high PM_{10} values, both in the fine and coarse fraction of particles. Interestingly, this flow type was not only associated with high ^{210}Pb values, but also with high ^{7}Be, which could be connected to the combination of African dust uplifting and subsidence from the upper troposphere.

The association of the seasonality of air mass transports with the seasonality of radionuclides and particulate matter has also been studied. In fact, while ^{7}Be winter maximum is related to the seasonal behaviour of Arctic and North-Atlantic air masses that reach Mt. Cimone after traversing the Alps, ^{7}Be summer maximum can be connected to the seasonal pattern of Mediterranean-Africa, Western and North Atlantic air masses. ^{210}Pb summer maximum is well

related with the seasonality of Western and North Western-Europe flows, whereas the seasonal pattern of PM_{10} might be, however, influenced by the seasonal pattern of advection types bringing about elevated mass loads of particles, such as Mediterranean-Africa, Western, North Atlantic and North Western-Europe flows.

Temporal trends were detected by means of non-parametric techniques applied on the monthly frequencies of flow types and on monthly medians: over the period 1999-2006, an upward trend for Arctic flows and a downward trend for Western flows reaching Mt. Cimone at 2200 m was detected. In addition, a downward trend for the monthly medians of ^{210}Pb and PM_{10} measured at the station, and a contemporary downward trend for WeMOi during the study period, possibly connected to the decreasing trend of Western flows, were also detected. The simultaneous decreasing trends of both ^{210}Pb and PM_{10} cannot be ascribed exclusively to a decrease in anthropogenic emissions, highlighting the potential influence exerted by meteorology, and suggesting further investigations. In particular, the observation of a positive correlation of ^{210}Pb and PM_{10} with Western air masses, showing a decreasing trend, and a negative correlation with Arctic flows, presenting an increasing trend, seems to largely explain the PM_{10} and ^{210}Pb trends observed in the time series. Significant upward temporal trends were detected for CO_2, in agreement with longer time records. The analysis of the magnitude of the seasonal and trend components of the monthly time series revealed that the largest variabilities in almost all the studied atmospheric variables are associated with the seasonal components, with a reduced weight of the trend component for all the series.

The association of teleconnection indices with advection pathways and atmospheric variables was also examined. In particular, positive associations of NAOi with the frequency of North-American, Atlantic and North-Atlantic flows, and between WeMOi and Western, Atlantic North-American and North-Atlantic flow types, were observed. The relationship between teleconnection indices and atmospheric variables highlight the significant influence of regional short scale modes of variability, like MO, over synoptic conditions and atmospheric conditions at the sampling site.

The results of this work highlight the role of flow pathways and teleconnections as factors that can have a deep influence in the variations in atmospheric composition at a site located in the central Mediterranean. This was possible since the time series of data acquired at the station was long enough to characterize a sort of short-term climatology of the site. The results are therefore of paramount importance to better understand processes controlling the variability of atmospheric composition in a region recognized as a hotspot of air pollution and climate change.

Acknowledgments and Data

The authors would like to gratefully thank Dr. Scott Chambers from ANSTO and an anonymous reviewer for providing constructive comments during the review process, which overall contributed to improve the quality of the manuscript. CAMM Monte Cimone by Italian Air Force and ISAC-CNR are gratefully acknowledged for their precious technical support at the Mt. Cimone station and for the help in the collection of compositional datasets, and in particular for providing data of meteorological and atmospheric composition data useful for this research. ISAC-CNR is gratefully acknowledged for providing aerosol size distribution, black carbon and ozone data, besides infrastructural access at the WMO-GAW Global Station Italian Climate Observatory "O. Vittori" at Mt. Cimone.
IAFMS is gratefully acknowledged for providing meteorological and carbon dioxide data.

World Data Centre for Greenhouse Gases (https://gaw.kishou.go.jp/) and EBAS databases (http://ebas.nilu.no/) are acknowledged for making available ozone, carbon dioxide, carbon monoxide, fine and coarse particle number density and black carbon data useful for this research work.
We acknowledge NOAA (http://www.esrl.noaa.gov/) for providing the HYSPLIT trajectory model (available at http://ready.arl.noaa.gov/HYSPLIT.php) and the NCEP/NCAR reanalysis data used in this study. NOAA/ESRL Physical Sciences Division, Boulder Colorado is also acknowledged for providing daily images of meteorological variables (available at http://www.esrl.noaa.gov/psd/) useful for this research.
The University of Wyoming (http://weather.uwyo.edu/upperair/sounding.html) and NASA Goddard Earth Sciences Data and Information Services Center (http://mirador.gsfc.nasa.gov) are acknowledged for providing soundings and satellite data.
James Hurrell and the National Center for Atmospheric Research staff are acknowledged for providing NAO indices (both station and Principal Component-based) data and metadata retrieved from https://climatedataguide.ucar.edu/climate-data/hurrell-north-atlantic-oscillation-nao-index-station-based.
Tim Osborn and CRU staff are acknowledged for providing NAO indices based on the difference between the sea level pressure over Gibraltar and the sea level pressure over Southwest Iceland retrieved from https://crudata.uea.ac.uk/cru/data/nao/
Erika Brattich thanks the University Miguel Hernandez de Elche and Prof. Orza for giving her the possibility of a three months research period to start the collaboration which posed the scientific basis of this work.
A description of the observational data used in this work is available in Sect. 2 and they are available upon request by contacting Prof. Laura Tositti (laura.tositti@unibo.it) for radionuclides observations, and by MOVIDA – Multistation system (http://shiny.bo.isac.cnr.it:3838/plot-multistats-en/), implemented under the Project of National Interest NextData) for other surface atmospheric variables observations.

References

Aebischer, U., & Schär, C., 1998. Low-Level Potential Vorticity and Cyclogenesis to the Lee of the Alps. Journal of the Atmospheric Sciences, 55, 186-207. doi:10.1175/1520-14691998055<0186:LLPVAC>2.0.CO;2

Añel, J.A., Gimeno, L., de la Torre L., & Nieto, R., 2006. Changes in tropopause height for the Eurasian region determined from CARDS radiosonde data. Naturwissenschaften, 93, 603-609. doi:10.1007/s00114-006-0147-5

Angulo-Martínez, M., & Beguería, S., 2012. Do atmospheric teleconnection patterns influence rainfall erosivity? A study of NAO, MO and WeMO in NE Spain, 1955-2006. Journal of Hydrology, 450-451, 168-179. doi:10.1016/j.jhydrol.2012.04.063

Arimoto, R., Snow, J.A., Graustein, W.C., Moody, J.L., Ray, B.J., Duce, R.A., Turekian, K.K., & Maring, H.B., 1999. Influences of atmospheric transport pathways on radionuclide activities in aerosol particles from over the North Atlantic. Journal of Geophysical Research, 104, D17, 301-321. doi:10.1029/1999JD900356

Balkanski, Y.J., Jacob, D.J., Gardner, G.M., Graustein, W.C., & Turekian, K.K., 1993. Transport and residence times or tropospheric aerosols inferred from a global three-dimensional simulation of ^{210}Pb. Journal of Geophysical Research, 98, 20573-20586. doi:10.1029/93JD02456

Barmpadimos, I., Hueglin, C., Keller, J., Henne, S., & Prévôt, A.S.H., 2011. Influence of meteorology on PM_{10} trends and variability in Switzerland from 1991 to 2008. Atmospheric Chemistry and Physics, 11, 1813-1835. doi:10.5194/acp-11-1813-2011

839 Barmpadimos, I., Keller, J., Oderbolz, D., Hueglin, C., & Prévôt A.S.H., 2012. One decade of parallel
840 fine $PM_{2.5}$ and coarse PM_{10}-$PM_{2.5}$ particulate matter measurements in Europe: trends and variability.
841 Atmospheric Chemistry and Physics, 12, 3189-3203. doi:10.5194/acp-12-3189-2012

842 Barnston, A.G., & Livezey, R.E., 1987. Classification, seasonality and persistence of low-frequency
843 atmospheric circulation patterns. Monthly Weather Review 115, 1083-1126.

844 Baskaran, M., 2011. Po-210 and Pb-210 as atmospheric tracers and global atmospheric Pb-210 fallout: a
845 review. Journal of Environmental Radioactivity, 102, 500-513. doi:10.1175/1520-
846 04931987115<1083:CSAPOL<2.0.CO;2

847 Beer, J., McCracken, K., & von Steiger, R., 2012. Cosmogenic radionuclides. Springer, Heidelberg, pp.
848 428.

849 Beine, H.J., Amoroso, A., Esposito, G., Sparapani, R., Ianniello, A., Georgiadis, T., Nardino, M.,
850 Bonasoni, P., et al. 2005. Deposition of atmospheric nitrous acid on alkaline snow surfaces.
851 Geophysical Research Letters, 32, L10808. doi:10.1029/2005GL022589

852 Bonasoni, P., Evangelisti, F., Bonafé, U., Feldmann, H., Memmesheimer, M., Stohl, A., & Tositti, L.,
853 1999. Stratosphere-troposphere exchanges: case studies recorded at Mt. Cimone during VOTALP
854 project. Physics and Chemistry of the Earth, Part C: Solar, Terrestrial and Planetary Science, I 245,
855 443-446. doi:10.1016/S1464-19179900069-0

856 Bonasoni, P., Stohl, A., Cristofanelli, P., Calzolari, F., Colombo, T., & Evangelisti, F., 2000a.
857 Background ozone variations at Mt Cimone station. Atmospheric Environment, 34, 5183-5189.
858 doi:10.1016/S1352-23100000268-5

859 Bonasoni, P., Evangelisti, F., Bonafé, U., Ravegnani, F., Calzolari, F., Stohl, A., Tositti, L., Tubertini, O.,
860 et al. 2000b. Stratospheric ozone intrusion episodes recorded at Mt. Cimone during VOTALP
861 project: Case studies. Atmospheric Environment, 34, 1355-1365. doi:10.1016/S1352-23109900280-0

862 Brankov, E., Rao, S.T., & Porter, P.S., 1998. A trajectory-clustering correlation methodology for
863 examining the long-range transport of air pollutants. Atmospheric Environment 32 9, 1525-1534.
864 doi:10.1016/S1352-23109700388-9

865 Brattich, E., Hernández-Ceballos, M.A., Cinelli, G., & Tositti L., 2015a. Analysis of ^{210}Pb peak values at
866 Mt. Cimone 1998-2011. Atmospheric Environment, 112, 136-147.
867 doi:10.1016/j.atmosenv.2015.04.020

868 Brattich, E., Riccio, A., Tositti, L., Cristofanelli, P., & Bonasoni, P., 2015b. An outstanding Saharan Dust
869 event at Mt. Cimone 2165 m asl, Italy in March 2004. Atmospheric Environment, 113, 223-235.
870 doi:10.1016/j.atmosenv.2015.05.017

871 Brattich, E., Hernández-Ceballos, M.A., Orza, J.A.G., Bolívar, J.P., & Tositti, L., 2016. The western
872 Mediterranean basin as an aged aerosols reservoir: insights from an old-fashioned but efficient
873 radiotracer. Atmospheric Environment, 141, 481-493. doi:10.1016/j.atmosenv.2016.07.022

874 Brattich, E., Orza, J.A.G., Cristofanelli, P., Bonasoni, P., & Tositti, L., 2017a. Influence of stratospheric
875 air masses on radiotracers and ozone over the central Mediterranean. Journal of Geophysical
876 Research: Atmospheres, 12213, 7164-7182. doi:10.1002/2017JD027036

877 Brattich, E., Liu, H., Tositti, L., Considine, D.B., & Crawford, J.H., 2017b. Processes controlling the
878 seasonal variations in ^{210}Pb and ^{7}Be at the Mt. Cimone WMO-GAW global station, Italy: a model
879 analysis. Atmospheric Chemistry and Physics, 17, 1061-1080. doi:10.5194/acp-17-1061-2017

880 Brunetti, M., Maugeri, M., & Nanni, T., 2002. Atmospheric circulation and precipitation in Italy for the
881 last 50 years. International Journal of Climatology, 22, 1455-1471. doi:10.1002/joc.805

Bueh, C., & Nakamura, Y., 2007. Scandinavian pattern and its climatic impact. Quarterly Journal of the Royal Meteorological Society, 133, 2117-2131, doi:10.1002/qj.173

Cabello, M., Orza, J.A.G., & Galiano, V., 2008a. Influence of meteorological input data on backtrajectory cluster analysis-a seven-year study for southeastern Spain. Advances in Science and Research, 2, 65-70. doi:10.5194/asr-2-65-2008

Cabello, M., Orza, J.A.G., & Galiano, V., 2008b. Air mass origin and its influence over the aerosol size distribution: a study in SE Spain. Advances in Science and Research, 2, 47-52. doi:10.5194/asr-2-47-2008

Chambers, S.D., Zahorowski, W., Williams, A.G., Crawford, J., & Griffiths, A.D., 2013. Identifying tropospheric baseline air masses at Mauna Loa Observatory between 2004 and 2010 using Radon-222 and back trajectories. Journal of Geophysical Research Atmospheres, 118, doi:10.1029/2012JD018212

Chambers, S.D., Hong, S.-B., Williams, A.G., Crawford, J., Griffiths, A.D., & Park, S.-J., 2014. Characterising terrestrial influence on Antarctic air masses using Radon-222 measurements at King George Island. Atmospheric Chemistry and Physics, 14, 9903-9916, doi:10.5194/acpd-14-11541-2014

Chambers, S.D., Williams, A.G., Conen, F., Griffiths, A.D., Reimann, S., Steinbacher, M., Krummel, P.B., Steele, L.P., van der Shoot, M.V., Galbally, I.E., Molloy, S.B., & Barnes, J.E., 2016a. Towards a universal "baseline" characterization of air masses for high- and low-altitude observing stations using 'Radon-222'. Aerosol and Air Quality Research, 16, 885-899, doi:10.4209/aaqr.2016.06.0391

Chambers, S.D., Kang, C.-H., Williams, A.G., Crawford, J., et al., 2016b. Improving the representation of cross-boundary transport of anthropogenic pollution in East Asia using Radon-222. Aerosol and Air Quality Research 16, 958-976, doi:10.4209/aar.2015.08.0522

Ciattaglia, L., 1983. Interpretation of Atmospheric CO_2 measurements at Mt. Cimone Italy Related to Wind Data. Journal of Geophysical Research, 88, C2, 1331-1338. doi:10.1029/JC088iC02p01331

Ciattaglia, L., Cundari, V., & Colombo, T., 1987. Further measurements of atmospheric carbon dioxide at Mt. Cimone, Italy: 1979-1985. Tellus B, 39, 1-2, 13-20. doi:10.3402/tellusb.v39i1-2.15319

Cleveland, R.B., Cleveland, W.S., McRae, J.E., & Terpenning, I., 1990. STL: A seasonal-trend decomposition procedure based on Loess. Journal of Official Statistics 6, 3–73.

Colette, A., Granier, C., Hodnebrog, Ø., Jakobs, H., Maurizi, A., Nyiri, A., Bessagnet, B., D'Angiola, A., et al., 2011. Air quality trends in Europe over the past decade: a first multi-model assessment. Atmospheric Chemistry and Physics, 11, 11657-11678. doi:10.5194/acp-11-11657-2011

Colombo, T., Santaguida, R., Capasso, A., Calzolari, F., Evangelisti, F., & Bonasoni P., 2000. Biospheric influence on carbon dioxide measurements in Italy. Atmospheric Environment, 34, 4963-4969. doi:10.1016/S1352-231000000366-6

Conte, M., Giuffrida, S., & Tedesco, S., 1989. The Mediterranean oscillation: impact on precipitation and hydrology in Italy. In: Proceedings of the Conference on Climate and Water, Vol. 1. Publications of Academy of Finland: Helsinki, pp. 121-137.

Cristofanelli, P., Bonasoni, P., Collins, W., Feichter, J., Forster, C., James, P., Kentarchos, A., Kubik, P.W., et al. 2003. Stratosphere-to-troposphere transport: A model and method evaluation. Journal of Geophysical Research, 108, D12, 8525. doi:10.1029/2002JD002600

Cristofanelli, P., Bonasoni, P., Tositti, L., Bonafé, U., Calzolari, F., Evangelisti, F., Sandrini, S., & Stohl, A., 2006. A 6-year analysis of stratospheric intrusions and their influence on ozone at Mt. Cimone

925 2165 m above sea level. Journal of Geophysical Research, 111, D03306.
926 doi:10.1029/2005JD006553.

927 Cristofanelli, P., Bonasoni, P., Carboni, G., Calzolari, F., Casarola, L., Zauli Sajani, S., & Santaguida R.,
928 2007. Anomalous high ozone concentrations recorded at a high mountain station in Italy in summer
929 2003. Atmospheric Environment 41, 1383-1394. doi:10.1016/j.atmosenv.2006.10.017

930 Cristofanelli, P., Calzolari, F., Bonafé, U., Duchi, R., Marinoni, A., Roccato, F., Tositti, L., & Bonasoni,
931 P., 2009a. Stratospheric intrusion index SI^2 from baseline measurement data. Theoretical and
932 Applied Climatology, 97, 317-325. doi:10.1016/j.atmosenv.2006.10.017

933 Cristofanelli, P., Marinoni, A., Arduini, J., Bonafé, U., Calzolari, F., Colombo, T., Decesari, S., Duchi,
934 R., et al., 2009b. Significant variations of trace gas composition and aerosol properties at Mt.
935 Cimone during air mass transport from North Africa – contributions from wildfire emissions and
936 mineral dust. Atmospheric Chemistry and Physics, 9, 4603-4619. doi:10.5194/acp-9-4603-2009

937 Cristofanelli, P., & Bonasoni, P., 2009. Background ozone in the southern Europe and Mediterranean
938 area: Influence of the transport processes. Environmental Pollution, 157, 1399-1406.
939 doi:10.1016/j.envpol.2008.09.017

940 Cristofanelli P., Fierli, F., Marinoni, A., Calzolari, F., Duchi, R., Burkhart, J., Stohl, A., Maione, M., et
941 al., 2013. Influence of biomass burning and anthropogenic emissions on ozone, carbon monoxide
942 and black carbon at the Mt. Cimone WMO-GAW global station Italy, 2165 m asl. Atmospheric
943 Chemistry and Physics, 13, 15-30. doi:10.5194/acp-13-15-2013

944 Cristofanelli P., Scheel, H.-E., Steinbacher, M., Saliba, M., Azzopardi, M., Ellul, R., Fröhlich, M., et al.,
945 2015. Long-term surface O_3 variability at Mt. Cimone WMO/GAW global station 2165 m asl, Italy.
946 Atmospheric Environment, 101, 23-33. doi:10.1016/j.atmosenv.2014.11.012

947 Cristofanelli, P., Landi, T.C., Calzolari, F., Duchi, R., Marinoni, A., Rinaldi, M., and Bonasoni, P., 2016.
948 Summer atmospheric composition over the Mediterranean basin: investigation on transport processes
949 and pollutant export to the free troposphere by observations at the WMO/GAW Mt. Cimone global
950 station Italy, 2165 m a.s.l. Atmospheric Environment, 141, 139-152,
951 doi:10.1016/j.atmosenv.2016.06.048

952 Cristofanelli, P., Busetto, M., Calzolari, F., Ammoscato, I., Gullì, D., Dinoi, A., Calidonna, C.R., Contini,
953 D., et al., 2017. Investigation of reactive gases and methane variability in the coastal boundary layer
954 of the central Mediterranean basin. Elementa Science of the Anthropocene, 5, 12,
955 doi:10.1525/elementa.216

956 Cristofanelli, P., Brattich, E., Decesari, S., Landi, T.C., Maione, M., Putero, D., Tositti, L., & Bonasoni
957 P., 2018. High-Mountain Atmospheric Research The Italian Mt. Cimone WMO/GAW Global Station
958 2165 m asl. SpringerBriefs in Meteorology ISBN 978-3-319-61126-6, doi:10.1007/978-3-319-
959 61127-3

960 Cuevas, E., Gonzalez, Y., Rodríguez, S., Guerra, J.C., Gómez-Peláez, A.J., Alonso-Pérez, S., Bustos, J.,
961 & Milford, C., 2013. Assessment of atmospheric processes driving ozone variations in the
962 subtropical North Atlantic free troposphere. Atmospheric Chemistry and Physics, 13, 1973-1998.
963 doi:10.5194/acp-13-1973-2013

964 Draxler, R., & Hess, G.D., 1997. Description of the HYSPLIT_4 modeling system. NOAA Tech. Memo.
965 ERL ARL-224 NOAA Air Resources Laboratory, Silver Spring, MD, 24 pp.

966 Draxler, R.R., & Hess, G.D., 1998. An overview of the HYSPLIT_4 modeling system of trajectories,

967 dispersion, and deposition. Australian Meteorological Magazine, **47**, 295-308.

Draxler, R.R., Stunder, B., Rolph, G., Stein, A., & Taylor, A., 2018. HYSPLIT4 user's guide, Version 4. NOAA Air Resources Laboratory. Last revised February 2018, https://www.arl.noaa.gov/document/reports/hysplit_user_guide.pdf Last accessed 11 November 2019

Duchi, R., Cristofanelli, P., Landi, T.C., Arduini, J., Bonafe, U., Bourcier, L., Busetto, M., Calzolari, F., Marinoni, A., Putero, D., and Bonasoni, P., 2016. Long-term 2002-2012 investigation of Saharan dust transport events at Mt. Cimone GAW global station, Italy 2165 m a.s.l. Elementa Science of the Anthropocene, 4, p.000085, doi:10.12952/journal.elementa.000085

Dueñas, C., Orza, J.A.G., Cabello, M., Fernández, M.C., Cañete, S., Pérez, M., & Gordo E., 2011. Air mass origin and its influence on radionuclide activities ^{7}Be and ^{210}Pb in aerosol particles at a coastal site in the western Mediterranean. Atmospheric Research, 101, 205-214. doi:10.1016/j.atmosres.2011.02.011

Dulac, F., Hamonou, E., Afif, C., Alkama, R., Ancona, C., Annesi-Maesano, I., Beekmann, M. & Benaissa, F., Bergametti, G., Boissard, C., Borbon, A., Bouet, C., 2016. Air quality and climate in the Mediterranean region. 10.4000/books.irdeditions.24600.

Feely, H.W., Larsen, R.J., & Sanderson, C.G., 1989. Factors that cause seasonal variations in ^{7}Be concentrations in surface air. Journal of Environmental Radioactivity, 9, 223-249. doi:10.1016/0265-931X-8990046-5

Fischer, H., Kormann, R., Klüpfel, T., Gurk, Ch., Königstedt, R., Parchatka, U., Mühle, J., Rhee, T.S., et al. 2003. Ozone production and trace gas correlations during the June 2000 MINATROC intensive measurement campaign at Mt Cimone. Atmospheric Chemistry and Physics, 3, 725-738. doi:10.5194/acp-3-725-2003

Fleming, Z.L., Monks, P.S., & Manning, A.J., 2012. Review: Untangling the influence of air-mass history in interpreting observed atmospheric composition. Atmospheric Research, 104-105, 1-39. doi:10.1016/j.atmosres.2011.09.009

Gaffney, J.S, Marley, N., & Cunningham, M.M., 2004. Natural radionuclides in fine aerosols in the Pittsburgh area. Atmospheric Environment, 38, 3191-3200. doi:10.1016/j.atmosenv.2004.03.015

Gordo, E., Liger, E., Dueñas, C., Fernandez, M., Cañete, S., & Pérez, M., 2015. Study of ^{7}Be and ^{210}Pb as radiotracers of African intrusions in Malaga Spain. Journal of Environmental Radioactivity, 148, 141-153. doi:10.1016/j.envrad.2015.06.028

Griffiths, A.D., Conen, F., Weingartner, E., Zimmermann, L., Chambers, S.D., Williams, A.G., & Steinbacher, M., 2014. Surface-to-mountaintop transport characterised by radon observations at the Jungfraujoch. Atmospheric Chemistry and Physics, 14, 12763-12779, doi:10.5194/acp-14-12763-2014

Grossi, C., Ballester, J., Serrano, I., Galmarini, S., Camacho, A., Curcoll, R., Morguí, J.A., Rodò, X., et al. 2016. Influence of long-range atmospheric transport pathways and climate teleconnection patterns on the variability of surface ^{210}Pb and ^{7}Be in southwestern Europe. Journal of Environmental Radioactivity, 165, 103-114, doi: 10.1016/j.jenvrad.2016.09.011

Hernández, F., Rodríguez, S., Karlsson, L., Alonso-Pérez, S., López-Pérez, M., Hernandez-Armas, J., & Cuevas, E., 2008. Origin of observed high ^{7}Be and mineral dust concentrations in ambient air on the Island of Tenerife. Atmospheric Environment 42, 4247-4256. doi:10.1016/j.atmosenv.2008.01.017

Hernandez-Ceballos, M.A., Brattich, E., and Cinelli, G., 2016. Heat-wave events in Spain: air mass analysis and impacts on ^{7}Be concentrations. Advances in Meteorology, 8026018, doi:10.115/2016/8026018

1012 Hirsch, R.M., Slack, J.R., & Smith, R.A., 1982. Techniques of trend analysis for monthly water quality
1013 data. Water Resources Research, 181, 107–121. doi:10.1029/WR018i001p00107

1014 Hurrell, J.W., 1995. Decadal trends in the North Atlantic oscillation: regional temperatures and
1015 precipitation. Science, 269, 676-679. doi:10.1126/science.269.5224.676

1016 Hurrell, J.W., 1996. Influence of variations in extratropical wintertime teleconnections on Northern
1017 Hemisphere temperatures. Geophysical Research Letters, 23, 665-668. doi:10.10.1029/96GL00459

1018 Hurrell, J.W., Deser, C., 2009. North Atlantic climate variability: the role of the North Atlantic Oscillation.
1019 Journal of Marine Systems, 78, 28-41.

1020 Hurrell, J.W., Kushnir, Y., Ottersen, G., & Visbeck, M., 2003. An overview of the North Atlantic Oscillation.
1021 In: The North Atlantic Oscillation: Climatic Significance and Environmental Impact, AGU monograph
1022 13, 1-35.

1023 Ioannidou, A., Vasileiadis, A., & Melas, D., 2014. Time lag between the tropopause height and ^{7}Be
1024 activity concentrations in surface air. Journal of Environmental Radioactivity 129, 80-85.
1025 doi:10.1016/j.jenvrad.2013.12.013

1026 Izquierdo, R., Alarcón, M., & Àvila, A., 2013. WeMO effects on the amount and the chemistry of winter
1027 precipitation in the north-eastern Iberian Peninsula. Tethys Journal of Weather and Climate of the
1028 Western Mediterranean, 10, 45-51. doi:10.3369/tethys.2013.10.05

1029 James, P, Stohl, A., Forster, C., Eckhardt, S., Seibert, P., & Frank, A., 2003. A 15-year climatology of
1030 stratosphere-troposphere exchange with a Lagrangian particle dispersion model 2. Mean climate and
1031 seasonal variability. Journal of Geophysical Research, 108D12, 8522. doi:10.1029/2002JD002639

1032 Jones, P.D., Jonsson, T., & Wheeler, D., 1997. Extension to the North Atlantic Oscillation using early
1033 instrumental pressure observations from Gibraltar and South-West Iceland. International Journal of
1034 Climatology, 17, 1433-1450. doi:10.1002/SICI1097-00881997111517:13<1433::AID-
1035 JOC203>3.0CO2-P

1036 Jorba, O., Pérez, C., Rocadenbosch, F., & Baldasano, J.M., 2004. Cluster analysis of 4-day back-
1037 trajectories arriving in the Barcelona Area, Spain, from 1997 to 2002. Journal of Applied
1038 Meteorology and Climatology, 43, 887-901. doi:10.1175/1520-
1039 04502004043<0887:CAODBT>2.0CO;2

1040 Kalnay E., Kanamitsu, M., Kistler, R., Collins, W., Deaven, D., Gandin, L., Iredell, M., Saha, S., et al.,
1041 1996. The NCEP/NCAR reanalysis 40-year project. Bulletin of the American Meteorological
1042 Society, 77, 437-471. doi:10.1175/1520-04771996077<0437:TNYRP>2.0.CO;2

1043 Koch, D.M., Jacob, J., & Graustein, W.C., 1996. Vertical transport of tropospheric aerosols as indicated
1044 ^{7}Be and ^{210}Pb in a chemical tracer model. Journal of Geophysical Research, 101: 18651-18666.
1045 doi:10.1029/96JD01176

1046 Kulan, A., Aldahan, A., Possnert, G., Vintersved, I., 2006. Distribution of ^{7}Be in surface air of Europe.
1047 Atmospheric Environment, 40, 3855-3868. doi:10.1016/j.atmosenv.2006.02.030

1048 Lee, H.N., Tositti, L., Zheng, X., & Bonasoni, P., 2007. Analyses and comparisons of variations of ^{7}Be,
1049 ^{210}Pb and ^{7}Be/^{210}Pb with ozone observations at two Global Atmosphere Watch stations from high
1050 mountains. Journal of Geophysical Research, 112, D05303. doi:10.1029/2006JD007421

1051 Li, Q., Jacob, D.J., Fairlie, T.D., Liu, H., Martin, R.V., & Yantosca, R.M., 2002. Stratospheric versus
1052 pollution influences on ozone at Bermuda: Reconciling past analyses. Journal of Geophysical
1053 Research, 107, D22, 4611. doi:10.1029/2002JD002138

Lim, Y.-K., 2015. The East Atlantic/West Russia EA/WR teleconnection in the North Atlantic: climate impact and relation to Rossby wave propagation. Climate Dynamics, 44, 11-12, 3211-3222, doi:10.1007/s00382-014-2381-4

Lozano, R.L., Hernández-Ceballos, M.A., San Miguel, E.G., Adame, J.A., & Bolívar, J.P., 2012. Meteorological factors influencing the ^{7}Be and ^{210}Pb concentrations in surface air from the southwestern Iberian Peninsula. Atmospheric Environment, 43, 168-178. doi:10.1016/j.atmosenv.2012.09.052

Machta, L., 1972. Mauna Loa and global trends in air quality. Bulletin of the American Meteorological Society, 53, 402-420. doi:10.1175/1520-04771972053<0402:MLAGTI>2.0.CO;2

Marinoni, A., Cristofanelli, P., Calzolari, F., Roccato, F., Bonafé, U., & Bonasoni, P., 2008. Continuous measurements of aerosol physical parameters at the Mt Cimone GAW Station 2165 m asl, Italy. Science of the Total Environment, 391, 241-251. doi:10.1016/j.scitotenv.2007.10.004

Martin-Vide, J., & Lopez-Bustins, J.-A., 2006. The Western Mediterranean Oscillation and rainfall in the Iberian Peninsula. International Journal of Climatology, 26, 1455-1475. doi:10.1002/joc.1388

Menut, L., Masson, O., & Bessagnet, R., 2009. Contribution of Saharan dust on radionuclide activity levels on Europe? The 21-22 February 2004 case study. Journal of Geophysical Research, 114, D16202. doi:10.1029/2009JD011767

Moulin, D., Lambert, C. E., Dulac, F., & Dayan, U., 1997. Control of atmospheric export of dust from North Africa by the North Atlantic Oscillation. Nature, 387, 691-694. doi:10.1038/42679

Myhre G., Shindell, D., Bréon, F.-M., Collins, W., Fugletsvedt, J., Huang, J., Koch, D., Lamarque, J.-F., et al., 2013. Anthropogenic and Natural Radiative Forcing. In: Climate Change 2013: The Physical Science Basis. Contribution of Working Group I to the Fifth Assessment Report of the Intergovernmental Panel on Climate Change. Stocker, T.F., Qin, D., Plattner, G.-K., Tignor, M., Allen, S.K., Boschung, J., Nauels, A., Xia, Y., et al. Eds. Cambridge University Press, Cambridge, United Kingdom and New York, NY, USA.

Ochoa-Hueso, R., Munzi, S., Alonso, R., et al., 2017. Ecological impacts of atmospheric pollution and interactions with climate change in terrestrial ecosystems of the Mediterranean basin: current research and future directions. Environmental Pollution, 227, 194-206, doi:10.1016/j.envpol.2017.04.062

Orza, J.A.G., Cabello, M., Galiano, V., Vermeulen, A.T., & Stein, A., 2013. The association between NAO and the interannual variability of the tropospheric transport pathways in western Europe. In: Lagrangian Modeling of the Atmosphere. Lin, J., Brunner, D., Gerbig, C., Stohl, A., Luhar, A., Webley, P. Eds. AGU Geophysical Monograph Vol. 200, 127-141.

Pace, G., Meloni, D., di Sarra, A., 2005. Forest fire aerosol over the Mediterranean basin during summer 2003. Journal of Geophysical Research 110, D21202. doi:10.1029/2005JD005986

Palutikof, J.P., 2003. Analysis of Mediterranean climate data: measured and modelled. In: Mediterraneean Climate-Variability and Trends. Bolle H.J. Ed.. Springer Verlag: Berlin; 133-153.

Papayannis, A., Amiridis, V., Mona, L., Tsaknakis, G., Balis, D., Bösenberg, J., Chaikovski, A., de Tomasi, F., et al., 2008. Systematic lidar observations of Saharan dust over Europe in the frame of EARLINET 2000-2002. Journal of Geophysical Research, 113, D10204. doi: 10.1029/2007JD009028.

Pausata, F.S.R., Pozzoli, L., Vignati, E., & Dentener, F.J., 2012. North Atlantic Oscillation and tropospheric ozone variability in Europe: model analysis and measurements intercomparison. Atmospheric Chemistry and Physics, 12, 6357-6376. doi:10.5194/acp-12-6357-2012

Pérez, N., Pey, J., Castillo, S., Viana, M., Alastuey, A., & Querol, X., 2008. Interpretation of the variability of levels of regional background aerosols in the Western Mediterranean. Science of the Total Environment, 407, 527-540. doi:10.1016/j.scitotenv.2008.09.006

Perrone, M.R., Becagli, S., Orza, J.A.G., Vecchi, R., Dinoi, A., Udisti, R., & Cabello, M., 2013. The impact of long-range-transport on PM1 and PM2.5 at a Central Mediterranean site. Atmospheric Environment, 71, 176-186. doi:10.1016/j.atmosenv.2013.02.006

Randerson, J.T., Thompson, M.V., Conway, T.J., Fung, I.Y., & Field, C.B., 1997. The contribution of terrestrial sources and sinks to trends in the seasonal cycle of atmospheric carbon dioxide. Global Biogeochemical Cycles, 114, 535-560. doi:10.1029/97GB02268

Santer, B.D., Painter, J.F., Bonfils, C., Mears, C.A., Solomon, S., Wigley, T.M.L., Glecker, P.J., Schmidt, G.A., et al. 2013. Human and natural influences on the changing thermal structure of the atmosphere. Proceedings of the National Academy of Sciences of the United States of America, 110, 43, 17235-17240. doi:10.1073/pnas.1305332110

Sarvan, D., Stratimirović, Đ., Blesić, S., Djurdjevic, V., Miljković, V., & Ajtić, J., 2017. Dynamics of beryllium-7 specific activity in relation to meteorological variables, tropopause height, teleconnection indices and sunspot number. Physica A, 469, 813-823, doi:10.1016/j.physa.2016.11.040

Seierstad, I.A., Stephenson, D.B., & Kvamsto, G., 2007. How useful are teleconnection patterns for explaining variability in extratropical storminess? Tellus Ser. A, 59, 170-181.

Stohl, A., Spoichtinger-Rakowsky, N., Bonasoni, P., Feldmann, H., Memmesheimer, M., Scheel, H.E., Trickl, T., Hübener, S., et al. 2000. The influence of stratospheric intrusions on alpine ozone concentrations. Atmospheric Environment, 34, 1323-1354. doi:10.1016/S1352-23109900320-9

Stohl, A., Haimberger, L., Scheele, M.P., & Wernli, H., 2001. An intercomparison of results from three trajectory models. Meteorological Applications, 8, 2, 127–135. doi:10.1017/S1350482701002018

Stohl A., Bonasoni, P., Cristofanelli, P., Collins, W., Feichter, W., Frank, A., Forster, C., Gerasopoulos, E., et al., 2003. Stratosphere-troposphere exchange: a review, and what we have learned from STACCATO. Journal of Geophysical Research, 108, D12, 8516. doi:10.1029/2002JD002490

Thoning, K.W., Tans, P.P., & Komhyr, W.D., 1989. Atmospheric carbon dioxide at Mauna Loa Observatory: 2. Analysis of the NOAA GMCC data, 1974-1985. Journal of Geophysical Research: Atmospheres, 94D6. DOI:10.1029/JD094iD06p08549

Tositti, L., Brattich, E., Cinelli, G., Previti, A., Mostacci, D., 2012. Comparison of radioactivity data measured in PM10 aerosol samples at two elevated stations in northern Italy during the Fukushima event. Journal of Environmental Radioactivity, 114, 105-112. doi:10.1016/j.jenvrad.2012.01.016

Tositti, L., Riccio, A., Sandrini, S., Brattich, E., Baldacci, D., Parmeggiani, S., Cristofanelli, P., & Bonasoni, P., 2013. Short-term climatology of PM10 at a high altitude background station in southern Europe. Atmospheric Environment, 65, 145-152. doi:10.1016/j.atmosenv.2012.10.051

Tositti, L., Brattich, E., Cinelli, G., Baldacci, D., 2014. 12 years of ^{7}Be and ^{210}Pb data in Mt. Cimone, and their correlation with meteorological parameters. Atmospheric Environment, 87C, 108-122. doi:10.1016/j.atmosenv.2014.01.014

Trigo, R., Xoplaki, E., Lüterbacher, J., Krichak, S.O., Alpert, P., Jacobeit, J., Sáenz, J., Fernández, J., González-Rouco, F., et al., 2006. Relations between variability in the Mediterranean region and mid-latitude variability. In: Mediterranean Climate Variability. Chapter 3, pp. 179-226. Lionello, P., Malanotte-Rizzoli, P., Boscolo, R. Eds. Elsevier, ISBN 978-0-444-52170-5. doi:10.1016/S1571-91970680006-6

Turekian, K.K., Nozki, Y., & Benninger, L.K., 1977. Geochemistry of atmospheric radon and radon products. Annual Review of Earth and Planetary Science, 5, 227-255.

Usoskin, I., & Kovaltsov, G., 2008. Production of cosmogenic ^{7}Be isotope in the atmosphere: full 3D modelling. Journal of Geophysical Research 113, D12107. doi:10.1029/2007JD009725

Yue, S., Pilon, P., Phinney, P., & Cavadias, G., 2002. The influence of autocorrelation on the ability to detect trend in hydrological series. Hydrological Processes 169, 1807-1829. doi:10.1002/hyp.1095

Wallace, J.M., & Gutzler, D.S., 1981. Teleconnections in the geopotential height field during the Northern Hemisphere winter. Monthly Weather Review, 109, 784-812.

Wilks, D., 2011. Statistical methods in the Atmospheric Sciences, Volume 100. International Geophysics Series. Third Edition Academic Press. ISBN-13: 978-0123850225

WMO World Meteorological Organization, 2007. Scientific Assessment on Ozone Depletion. 2006, Global Ozone Research Monitoring Project-Report, No.50, Geneva Switzerland.

WMO World Meteorological Organization-GAW Global Atmosphere Watch, 2017. WMO Greenhouse Gas Bulletin. The state of Greenhourse Gases in the Atmosphere Based on Global Observations through 2016. ISSN 2078-0796

Tables

Table 1. Analysed teleconnection with associated location of centers of action including the sign of geopotential height (or pressure) anomalies for their positive phases.

TELECONNECTION	ABBREVIATION	CENTERS OF ACTION
NORTH ATLANTIC OSCILLATION	NAO	Greenland (-), Azores (+)
EAST ATLANTIC	EA	North Atlantic (-), Subtropical North Atlantic and Mediterranean (+)
EAST ATLANTIC/WESTERN RUSSIA	EA/WR	NW Europe (+), Western Russia (-), NE China (+)
SCANDINAVIA	SCA	SW Europe (-), Scandinavia (+), Kazakhstan/Mongolia (-)
MEDITERRANEAN OSCILLATION	MO	Algiers (+), Cairo (-), Gibraltar (+), Israel (-)
WESTERN MEDITERRANEAN OSCILLATION	WeMO	Po Valley (-), Gulf of Cadiz (+)

Table 2. Results of the seasonal Kendall test for the monthly time series and the trend-free pre-whitening Yue-Pilon (Y-P) procedure on the de-seasonalized monthly series for the detection of monotonic trends applied on the 1999-2006 time series. For each case, the p (significance) value and the mean change per year from the Theil-Sen slope are presented. In bold when significant at the 0.05 level, in italic when the trend is only weakly significant, i.e., at the 0.1 level.

	MONTHLY FREQUENCIES			
	Seasonal Kendall		Deseasonalized Y-P	
INDEX	**p value**	**mean change per year**	**p value**	**mean change per year**
Hurrell_Stat_NAOi	0.6935	-0.07	0.3220	-0.08
Hurrell_PC_NAOi	0.2840	-0.05	0.3645	-0.05
CPC_Stat_NAOi	0.2110	-0.07	0.1307	-0.06
CRU_Stat_NAOi	0.4320	-0.07	0.4215	+0.04
WeMOi	**0.0000**	-0.15	**0.0000**	-0.17
MOi1	0.2530	+0.01	0.2497	+0.01
MOi2	0.6171	-0.01	0.1668	-0.01
EA	0.7206	+0.02	0.9028	+0.01
EA/WR	1.0000	-0.03	0.3612	-0.03
SCA	1.0000	+0.01	0.8875	+0.01
	Seasonal Kendall		**Deseasonalized Y-P**	
FLOW TYPE	**p value**	**mean change per year**	**p value**	**mean change per year**
A	**0.0383**	0.000	**0.0462**	+0.007
E	0.0760	+0.003	0.1358	+0.007
Me-AF	0.8284	+0.003	0.3924	+0.001
W	**0.0376**	-0.010	**0.0274**	-0.011
Atl	0.1061	-0.006	**0.0349**	-0.007
N-Am	0.0689	0.000	0.2872	-0.003
N-Atl	0.1605	-0.004	0.3462	-0.004
NW-Eu	0.7203	+0.003	0.9232	0.000
	Monthly medians			
	Seasonal Kendall		**Deseasonalized Y-P**	
VARIABLE	**p value**	**mean change per year**	**p value**	**mean change per year**
p (mbar)	0.1237	+0.317	0.2317	+0.133
T (°C)	0.1855	+0.300	0.1024	+0.168
RH (%)	0.1234	+0.263	0.4996	-0.336
TH (m)	0.7690	+19.296	0.9919	-10.414
ws (m s^{-1})	0.1336	+0.054	0.2292	+0.117
Prec (mm)	0.6408	+0.000	0.7777	+0.000
MixHeight (mm)	0.9083	+4.822	0.6875	-3.568
O_3 (ppbv)	0.1320	+0.279	0.1806	+0.292

CO_2 (ppm)	**0.0000**	+1.804	**0.0000**	+1.900
^{7}Be (mBq m^{-3})	0.2840	-0.079	0.1984	-0.085
^{210}Pb (mBq m^{-3})	**0.0450**	-0.008	**0.0135**	-0.011
PM_{10} (µg m^{-3})	**0.0053**	-0.154	**0.0083**	-0.296
$^{7}Be/PM_{10}$ (mBq μg^{-1})	0.1851	+0.007	0.1616	+0.012
^{210}Pb /PM_{10} (mBq μg^{-1})	0.7921	0.000	0.9839	+0.000
$^{7}Be/^{210}Pb$	0.6678	0.000	0.3612	+0.083

Figures

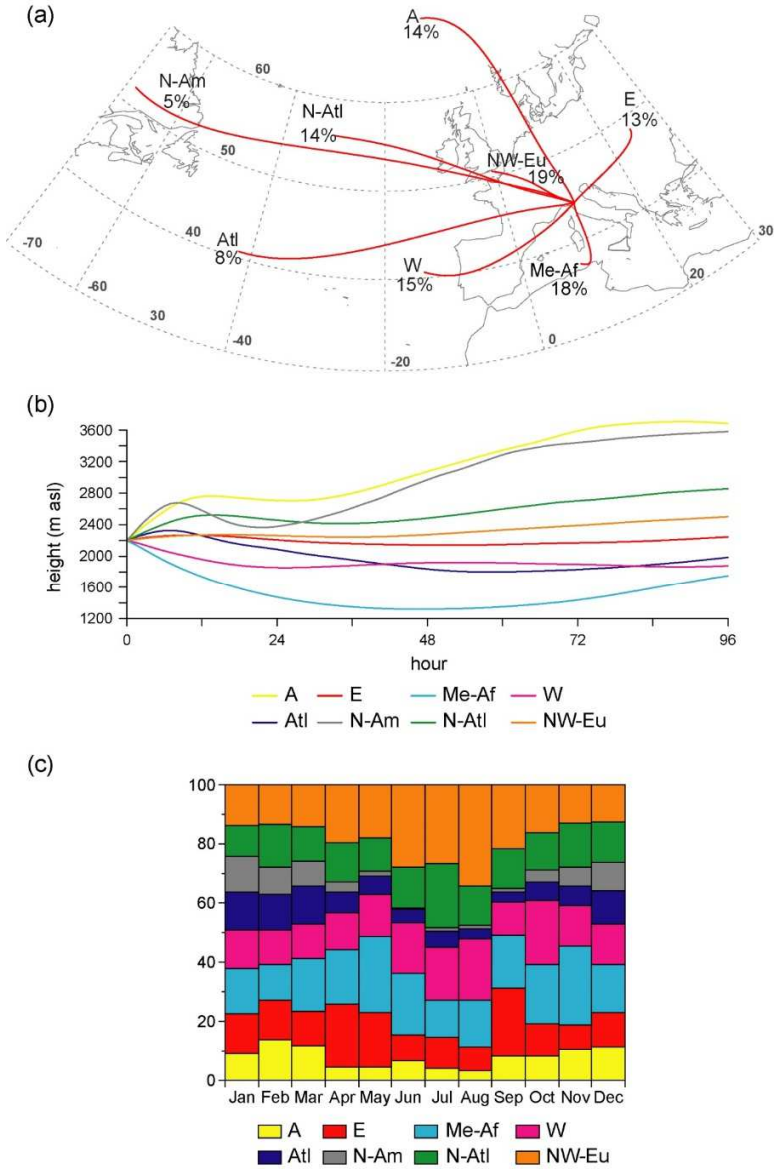

Figure 1. (a) Centroids of the trajectory clusters identified for 96-h back-trajectories arriving at 2200 m asl for the 12-year study period. The flow pathways are identified as follows: Arctic (A), Eastern (E), Mediterranean-Africa (Me-AF), Atlantic (Atl), Northern Atlantic (N-Atl), North America (N Am), North Western-Europe (NW-Eu). The percentage is for the frequency of occurrence of each flow pattern in the whole 1998-2011 period. (b) Heights above mean sea level of the representative back-trajectories vs. end-point time. (c) Monthly variation in percentage frequency of the identified advection pathways.

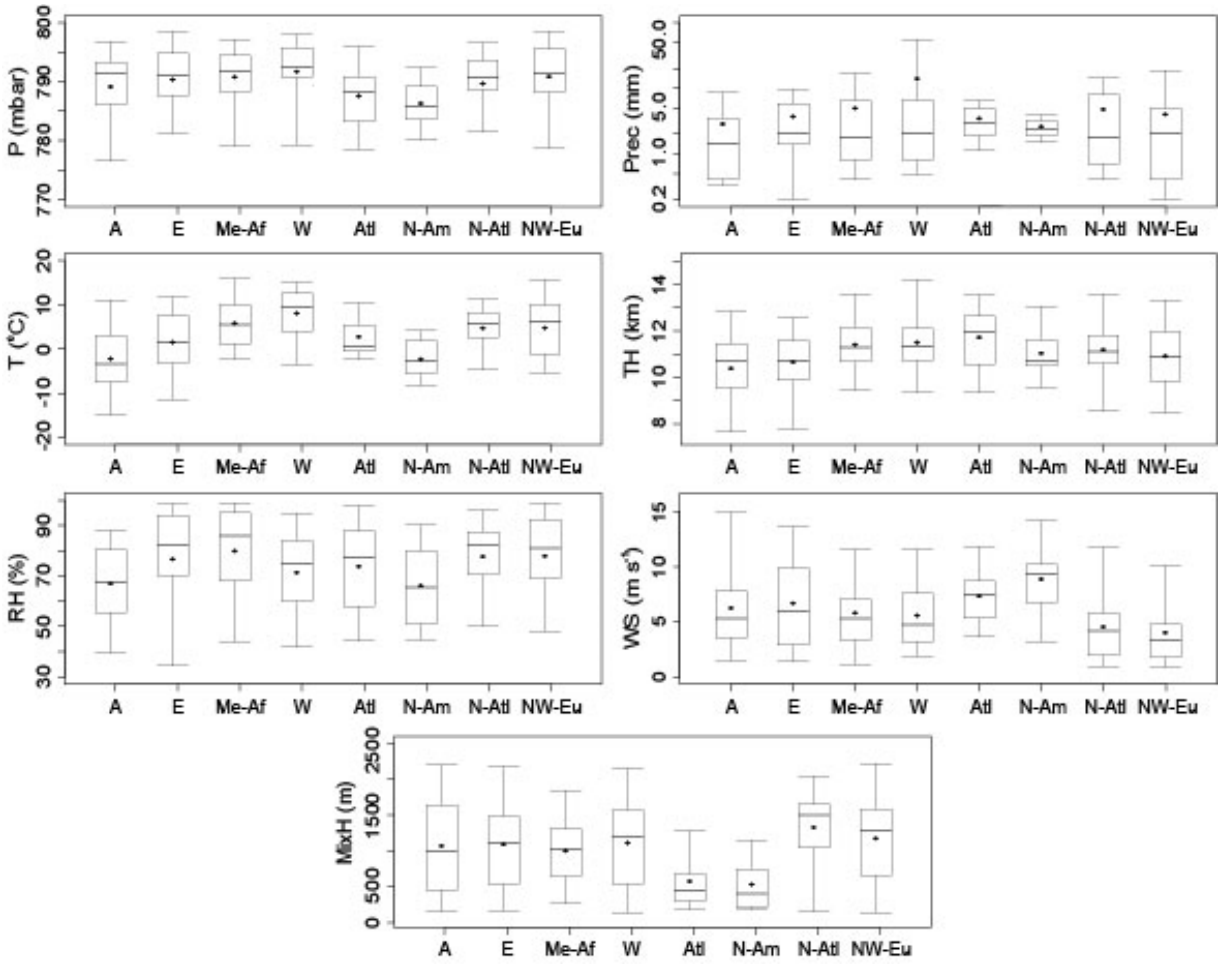

Figure 2. Box plots of meteorological variables measured at Mt. Cimone (P = pressure, T = temperature, RH = relative humidity, Prec = precipitation, TH = tropopause height, WS = wind speed, MixH = mixing height) versus air flows arriving at the receptor site. The horizontal bold line in each box represents the 50th percentile (median), the circle represents the mean value, lower and upper boundaries locate the 5th and 95th percentile of the values and whiskers locate the minimum and maximum values.

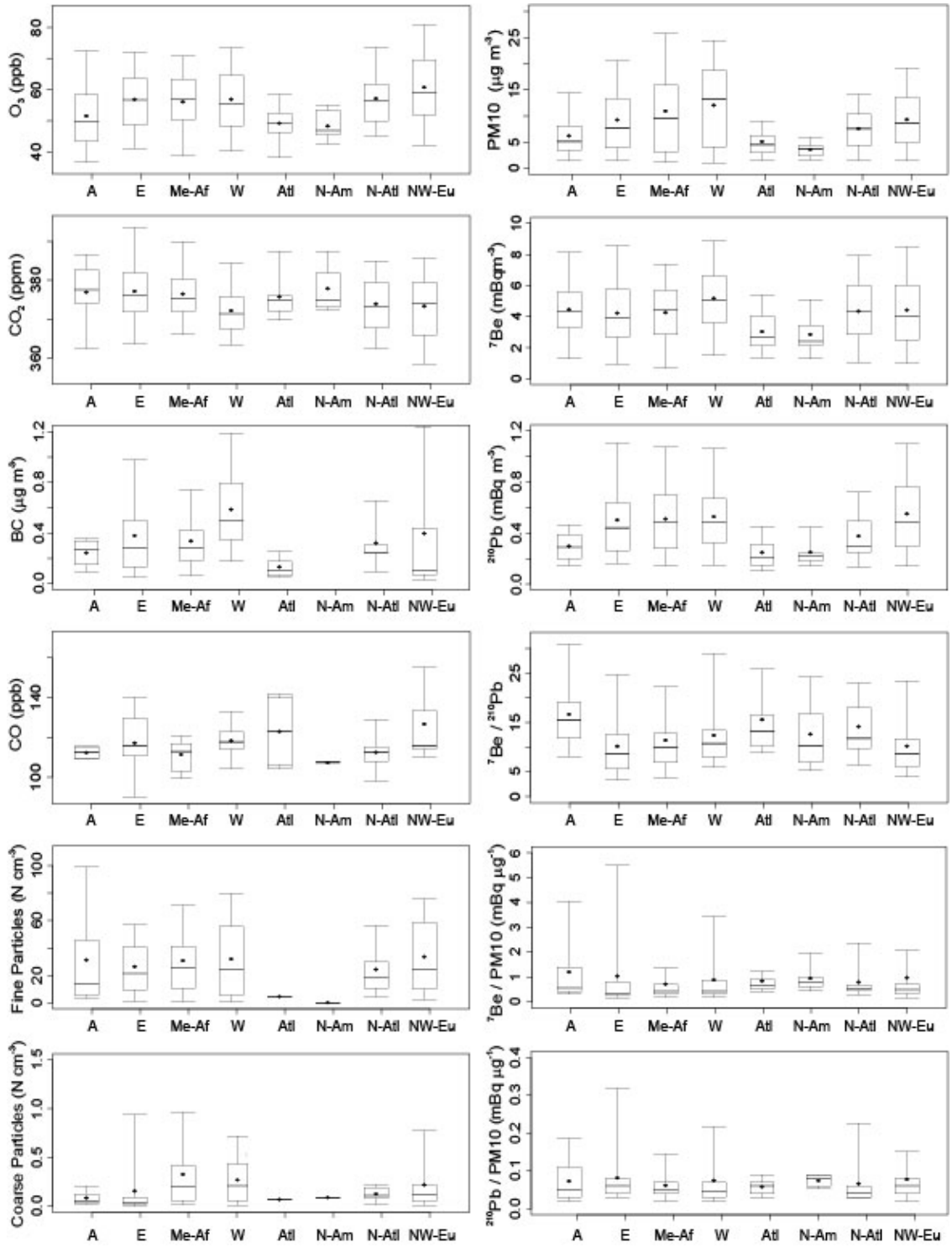

Figure 3. Same as Figure 2, but for atmospheric gases (O_3, CO_2, CO), black carbon (BC), fine and coarse particles number density, PM_{10}, atmospheric radiotracers ^{7}Be and ^{210}Pb, ratio $^{7}Be/^{210}Pb$, ratio $^{7}Be/PM_{10}$, ratio $^{210}Pb/PM_{10}$, versus air flows arriving at the receptor site.

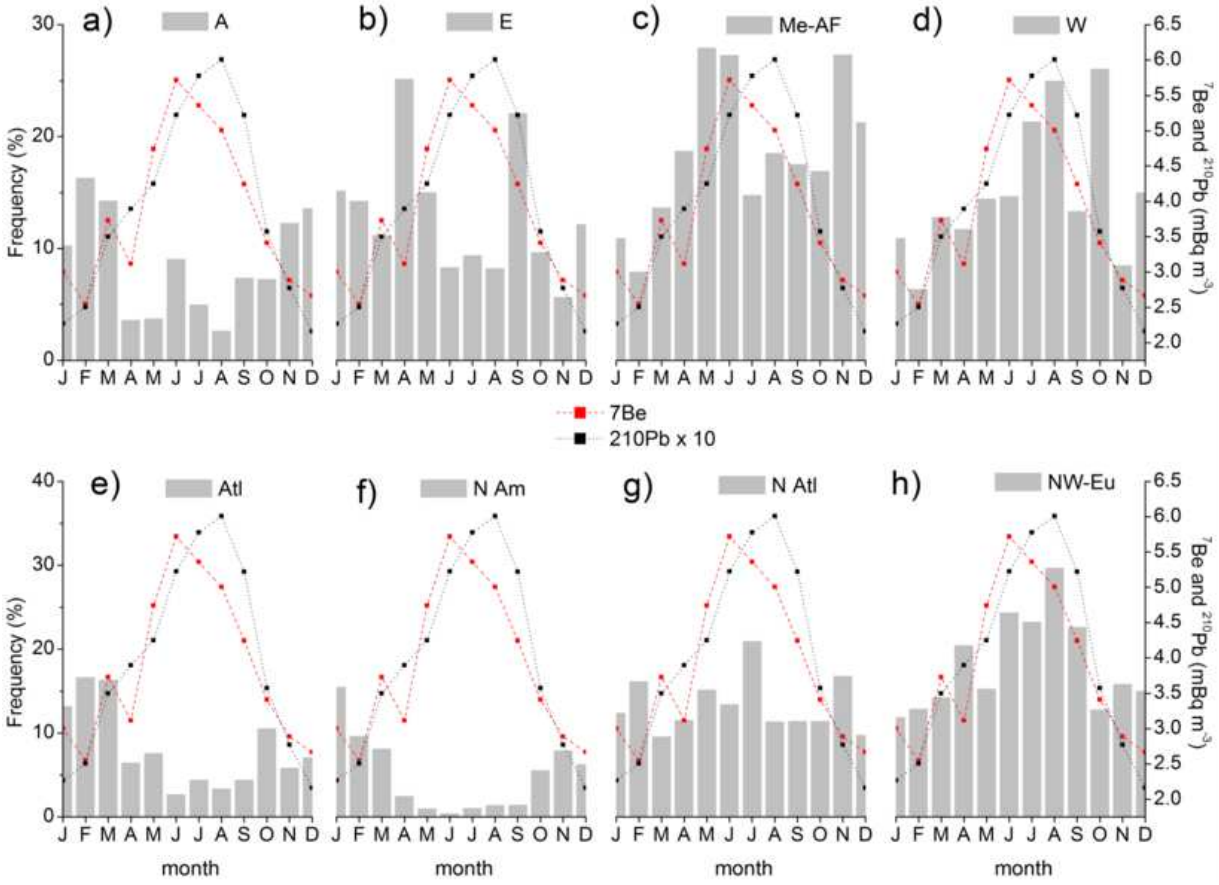

Figure 4. Monthly median activities of ^{7}Be (right scale, red line) and ^{210}Pb (right scale, black line) and their relationship with the monthly frequency of air flows (left scale, grey bar) at Mt. Cimone from: a) Arctic; b) East; c) Mediterranean-Africa; d) West; e) Atlantic; f) North America; g) North Atlantic; h) North Western-Europe

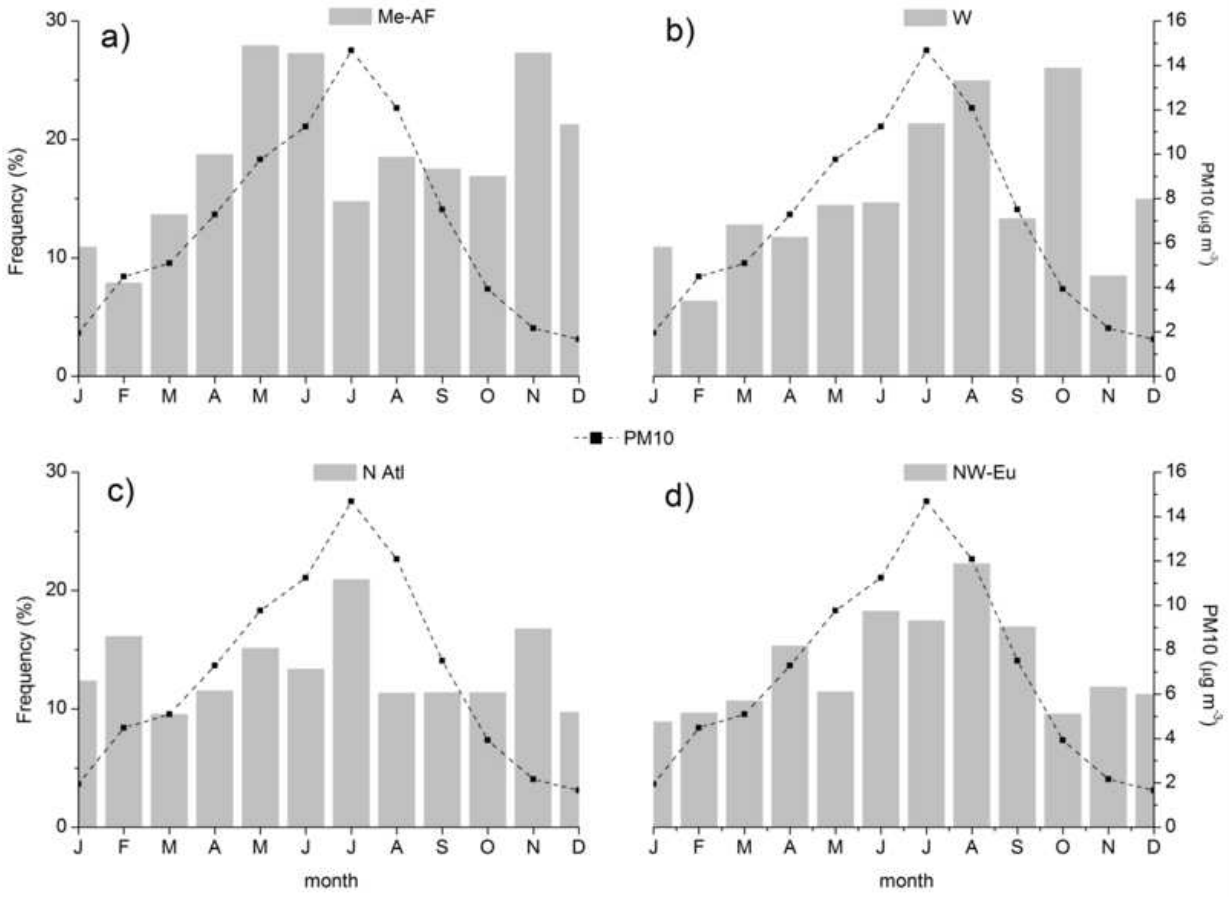

Figure 5. Monthly median concentrations of PM_{10} (right scale, black dashed line) and relationship with the monthly frequency of air flows (left scale, grey column) at Mt. Cimone from: a) Mediterranean-Africa; b) West; c) North Atlantic; d) North Western-Europe.

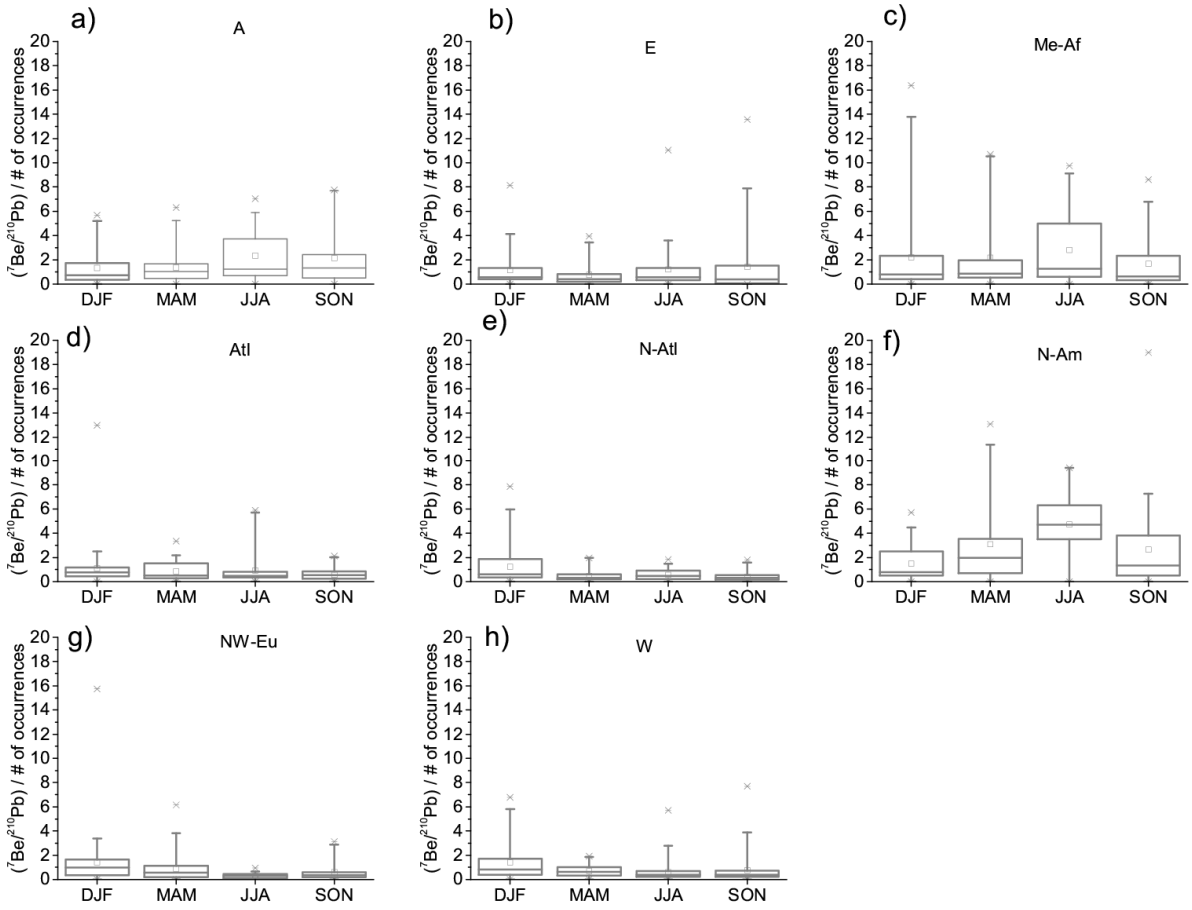

Figure 6. Seasonal (DJF = December-January-February; MAM = March-April-May; JJA = June-July-August; SON = September-October-November; i.e., winter, spring, summer and autumn seasons in the Northern Hemisphere) boxplots showing the contribution to ^{7}Be/^{210}Pb per number of events of each flow type: a) Arctic; b) Eastern; c) Mediterranean-Africa; d) Atlantic; e) North-Atlantic; f) North-America; g) North Western-Europe; h) Western. The horizontal bold line in each box represents the 50th percentile (median), the square represents the mean value, lower and upper boundaries locate the 25th and 75th percentile of the values and whiskers locate the 5th and 95th percentile values. Crosses and horizontal lines outside the boxes further indicate 1st and 99th percentile and minimum and maximum values, respectively.

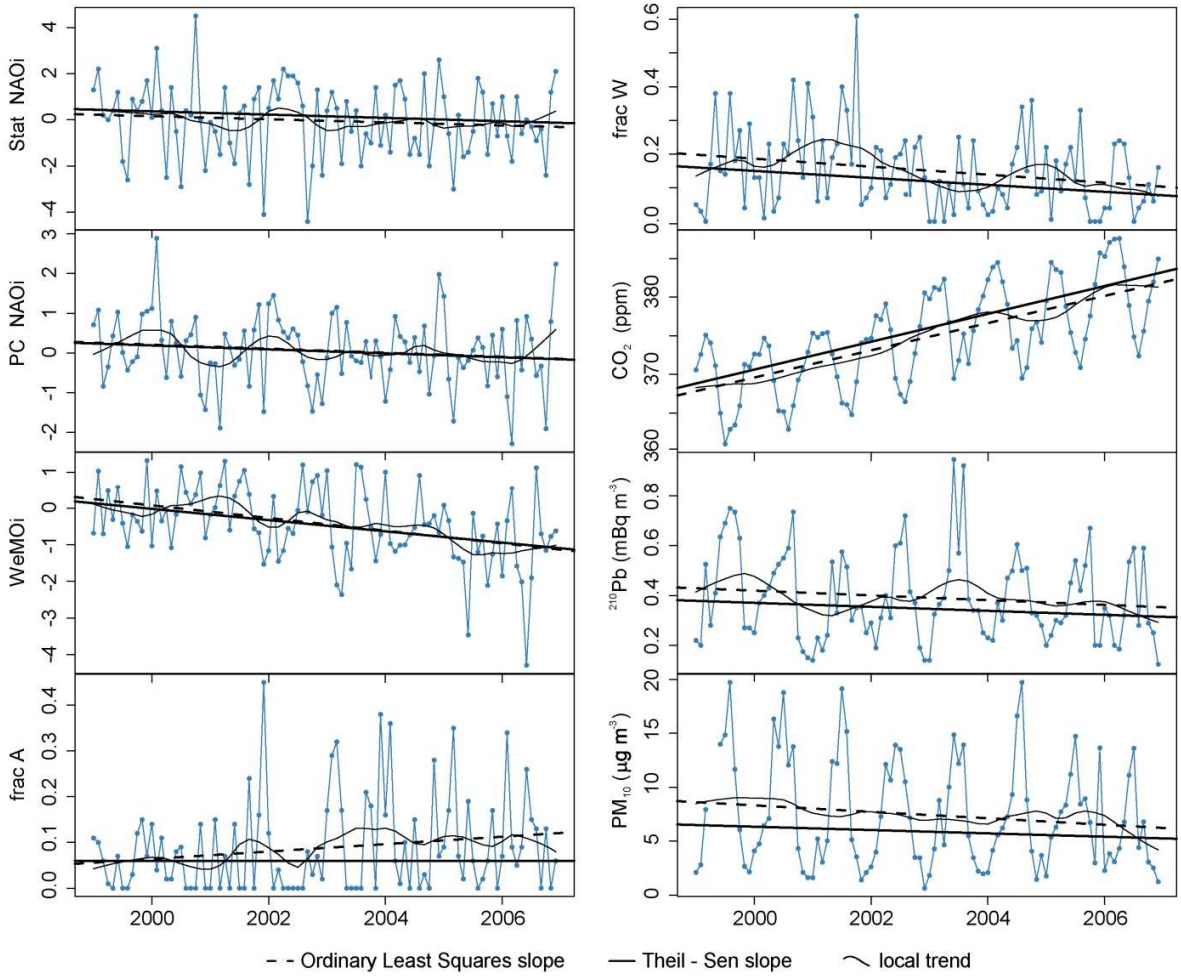

Figure 7. Evolution of the monthly frequency of occurrence of the Hurrell station- and principal components-based NAO, WeMO indices, of the Arctic and Western flow types, and of the monthly medians of variables which show significant trends, over the period 1999-2006 (CO_2, ^{210}Pb and PM_{10}). Dashed lines are the linear regressions, solid lines are the Theil-Sen slope estimates, and black solid curved lines are the local trends from the seasonal-trend decomposition analysis.

1321

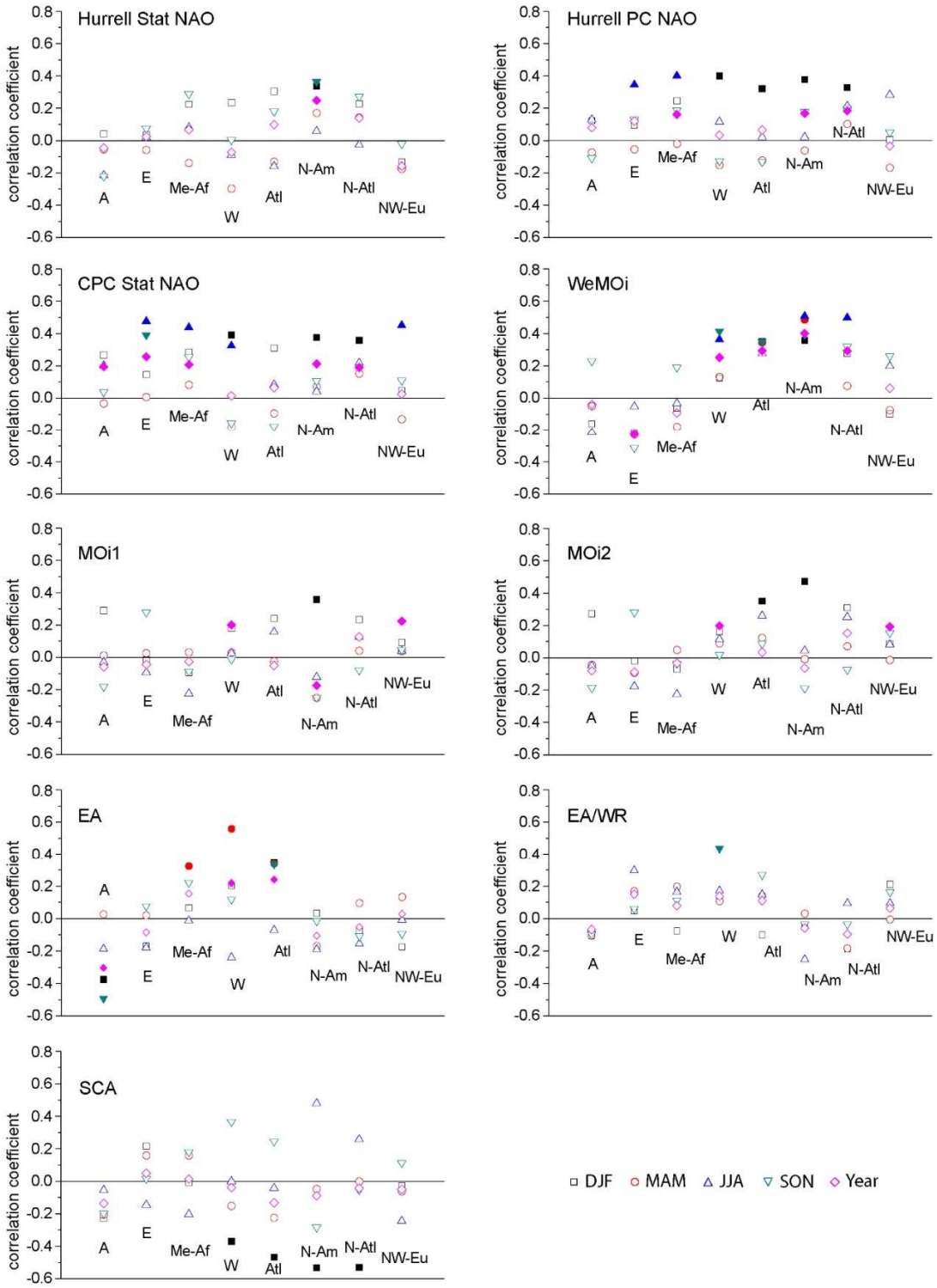
Hurrell Stat NAO
Hurrell PC NAO
CPC Stat NAO
WeMOi
MOi1
MOi2
EA
EA/WR
SCA
correlation coefficient
A
E
Me-Af
W
Atl
N-Am
N-Atl
NW-Eu
DJF
MAM
JJA
SON
Year

1322

Figure 8. Spearman correlation coefficients between the frequency of occurrence of the different teleconnection indices and air flow types by season and for the full year. Filled symbols indicate significant correlations ($p < 0.01$ significance level).

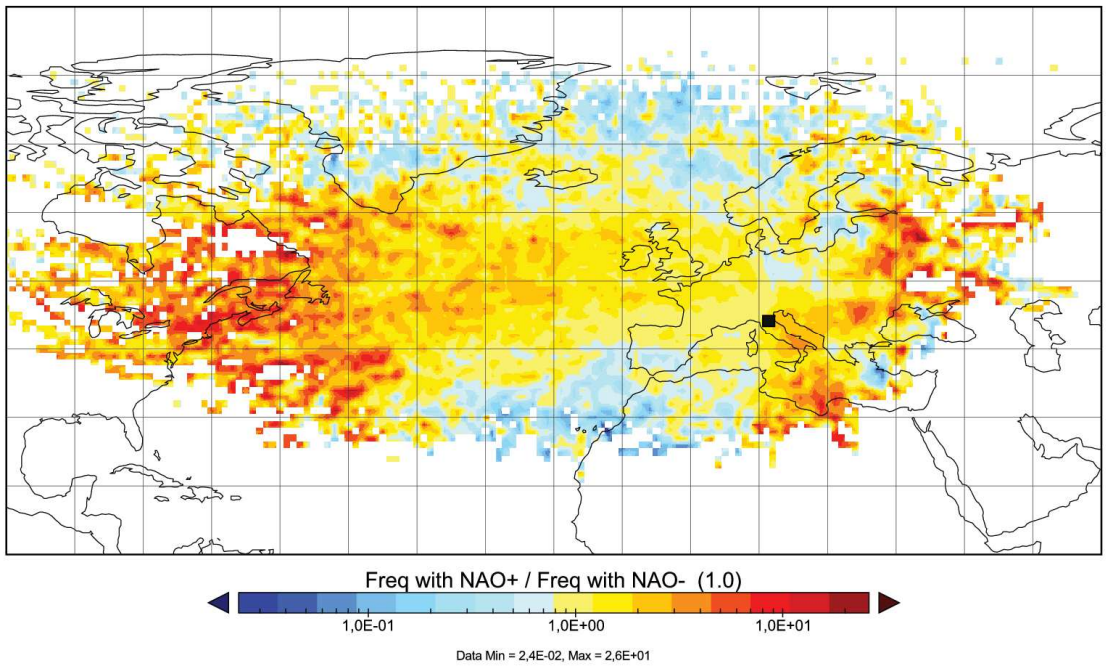

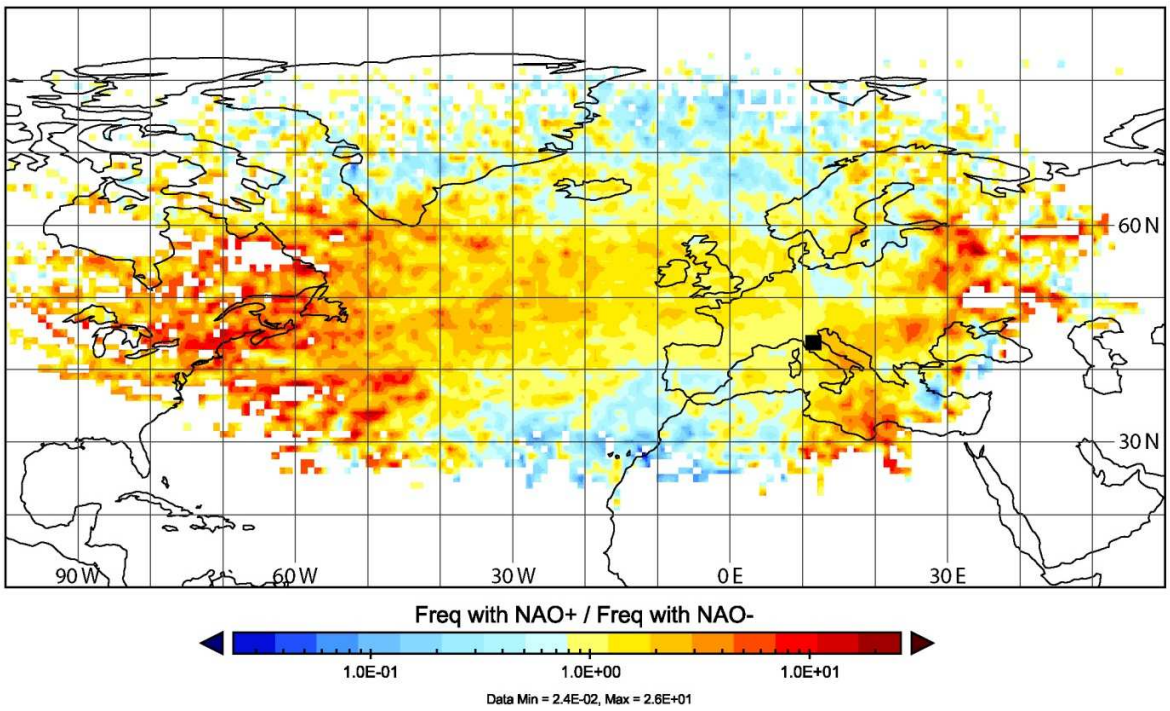

Figure 9. Ratio of residence time of air parcels reaching Mt. Cimone in the positive and negative phase of Hurrell Stat NAO (NAOi higher than +0.5 and lower than -0.5, respectively) in the extended winter DJFM period. The black dot indicates the position of Mt. Cimone.

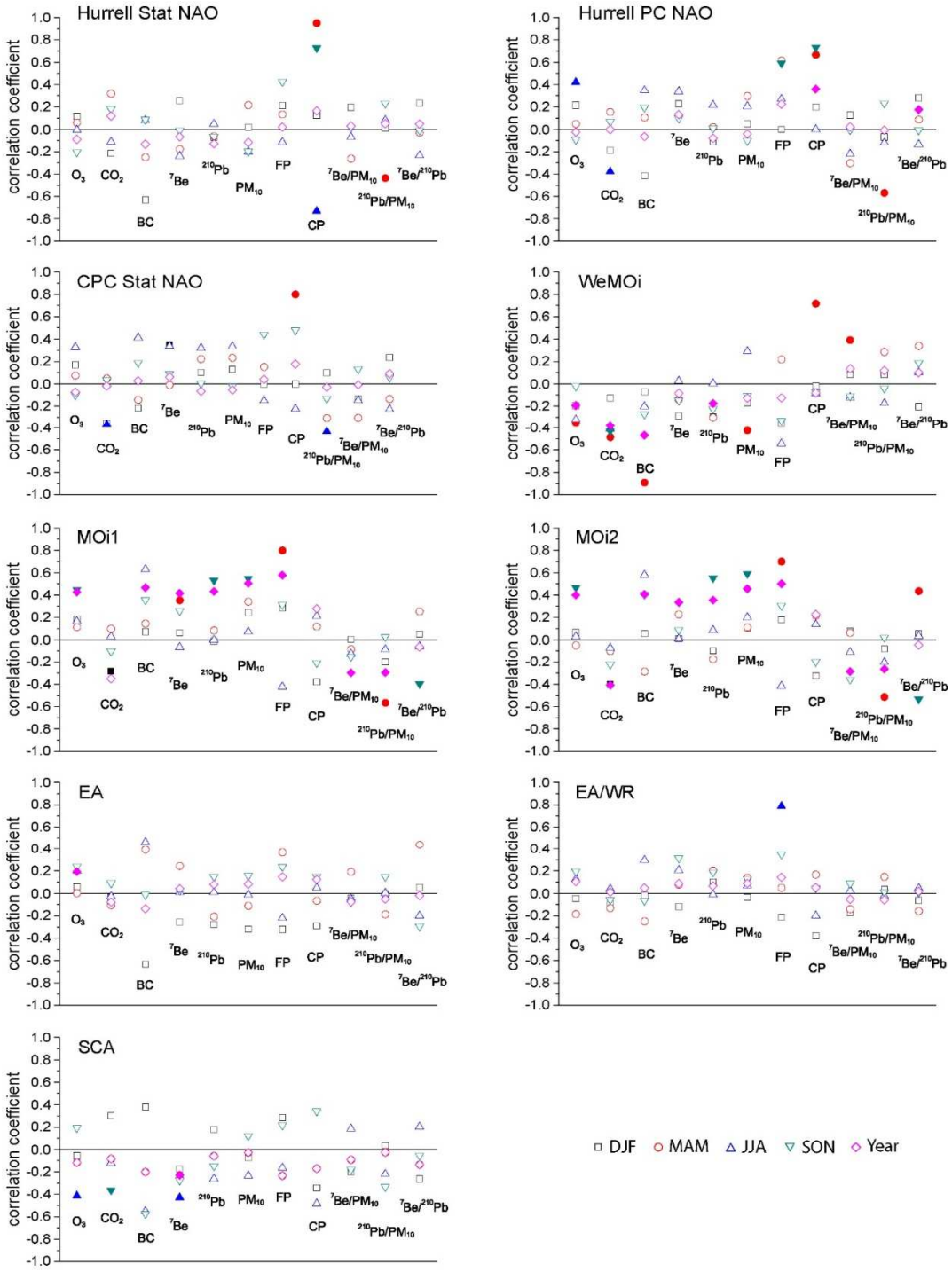

Figure 10. Spearman correlation coefficients between the teleconnection indices and the monthly medians of variables by season and for the full year. Filled symbols indicate significant correlations ($p < 0.01$ significance level) letters indicate the variables: O_3 = ozone, CO_2 = carbon dioxide, BC = black-carbon, ^{7}Be, ^{210}Pb, PM_{10}, FP = fine particles, CP = coarse particles, $^{7}Be/PM_{10}$, $^{210}Pb/PM_{10}$, $^{7}Be/^{210}Pb$.

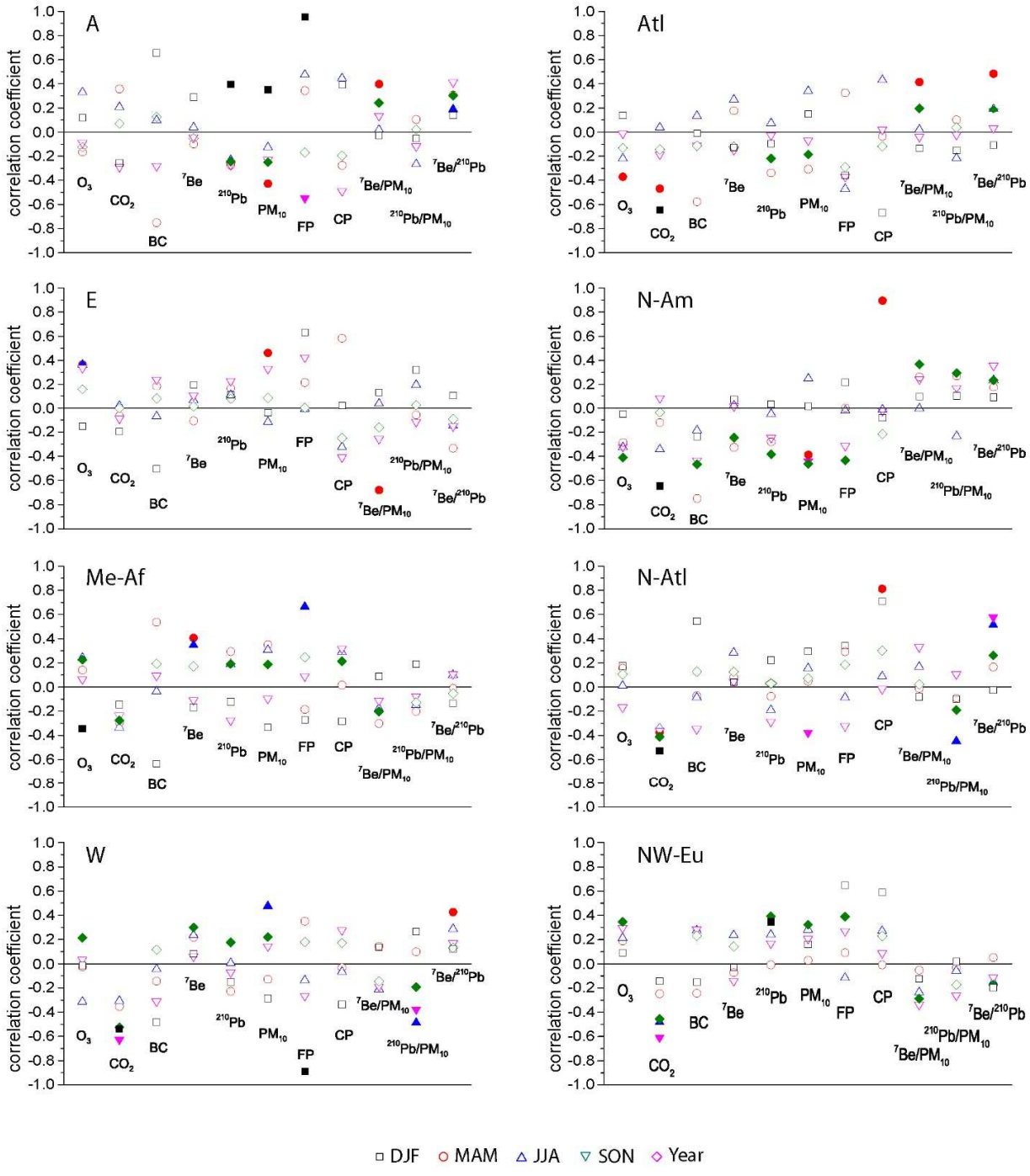

Figure 11. Same as Figure 10 but for the correlation between the frequency of occurrence of air flow types and the monthly medians of variables.